Journal of Drug Delivery Science and Technology 117 (2026) 108027

Contents lists available at ScienceDirect

Journal of Drug Delivery Science and Technology

journal homepage: www.elsevier.com/locate/jddst

A green strategy for resveratrol nanodelivery: A multidisciplinary approach for the physicochemical characterization of *Thymus*-based liposomes with anti-biofilm activity against *Listeria monocytogenes*

Maria Gioia Fabiano [a,1], Linda Maurizi [b,1], Jacopo Forte [a,c], Eleonora D'Intino [a], Maria Grazia Ammendolia [d], Davide Corinti [a], Astri D. Tagueha [e], Michela Relucenti [e], Orlando Donfrancesco [f], Federica Rinaldi [a,*], Maria Elisa Crestoni [a], Stefania Garzoli [a], Carlotta Marianecci [a], Maria Carafa [a,2], Catia Longhi [b,2]

[a] *Department of Drug Chemistry and technology, Sapienza University of Rome, Piazzale Aldo Moro 5, Rome, 00185, Italy*
[b] *Department of Public Health and Infectious Diseases, Microbiology Section, Sapienza University of Rome, Piazzale Aldo Moro 5, Rome, 00185, Italy*
[c] *Department of Basic Biotechnological Sciences, Intensivological and Perioperative Clinics, Catholic University of Sacred Heart, Largo Francesco Vito 1, 00168, Rome, Italy*
[d] *National Center of Innovative Technologies in Public Health, National Institute of Health, Rome, 00185, Italy*
[e] *Department of Anatomy, Histology, Forensic Medicine and Orthopedics, Section of Human Anatomy, Sapienza University of Rome, Via Alfonso Borelli 50, Rome, 00161, Italy*
[f] *Department of Life Science, Health and Health Professions, Link Campus University, Rome, 00165, Italy*

ARTICLE INFO

Keywords:
Liposomes
Listeria monocytogenes
Antibiofilm
Essential oil
GC/MS
HPLC-UV analysis
Electron microscopy

ABSTRACT

Nanocarrier-based drug delivery systems (DDS) offer promising strategies to enhance therapeutic efficacy, stability, and targeted delivery of bioactive compounds while reducing side effects. In this study, a multidisciplinary approach was employed to develop and characterize bioactive liposomes incorporating resveratrol (RV), a polyphenol with known therapeutic potential but limited bioavailability, and *Thymus vulgaris* essential oil (TEO), recognized for its antimicrobial and antioxidant properties. To obtain stable nanocarriers, liposomes were formulated using soy lecithin and prepared by thin layer evaporation technique followed by sonication process. To assess the preservation of TEO's chemical profile during formulation, Headspace Solid Phase Microextraction coupled with Gas Chromatography–Mass Spectrometry (HS-SPME/GC-MS) was performed. Quantitative analysis of thymol and carvacrol, the two main active components, was performed by HPLC-UV experiments. Physicochemical characterization of DDS was carried out employing Dynamic Light Scattering (DLS), UV–Vis spectrophotometer and Transmission electron microscopy. Antimicrobial activity was assessed by broth microdilution method, while biofilm inhibition ability was evaluated using crystal violet staining. The obtained nanocarriers exhibited appropriate physicochemical characteristics, including optimal particle size and stability. They can efficiently load both oil and RV. These features enhanced the antibacterial activity of LT-RV compared to free RV, and improved its inhibitory effect, at sub-MIC concentrations, against the sessile form of *Listeria monocytogenes* strains.

This study highlights the importance of integrating chemical, physical, and biological evaluations to develop effective nanocarrier-based formulations with the aim to identify a suitable strategy to combat infections associated with resistant, biofilm-producing pathogens, and offer a versatile and effective delivery platform.

* Corresponding author.
E-mail address: federica.rinaldi@uniroma1.it (F. Rinaldi).
[1] These authors contributed equally to this work.
[2] These authors jointly supervised this work.

https://doi.org/10.1016/j.jddst.2026.108027
Received 7 July 2025; Received in revised form 7 January 2026; Accepted 14 January 2026
Available online 21 January 2026

1. Introduction

Nanotechnology has emerged as a transformative field, particularly in the development of nanocarriers delivery systems that facilitate the targeted delivery of therapeutic agents and bioactive substances. The design of drug delivery systems (DDS) play a crucial role in formulating bioactive molecules into suitable forms, improving stability and therapeutic efficacy and minimizing side effects [1]. The choice of DDS components is crucial: they must be biocompatible, non-toxic and able to confer additional bioactivity and boost the efficacy of the encapsulated drug [2]. Essential oils (EOs) are well known for their broad spectrum of beneficial properties, including antimicrobial, anti-inflammatory, antioxidant, and anticancer activities. Moreover, EOs represent green natural safe and effective alternatives to chemical antimicrobial agents.

EOs are complex mixtures primarily composed of volatile terpenoids and phenolic compounds, which are susceptible to differential evaporation and chemical degradation, including oxidation and isomerization [3,4]. Such processes can lead to compositional changes, consequently altering their therapeutic potential. Therefore, ensuring their effective application over time, and long-term preservation, is crucial to optimizing the use of EOs. In this regard, DDS is an effective means to stabilize EOs, especially for the protective effect of polymeric drug carriers [5].

Determining their complex chemical composition plays a key role in understanding how the metabolite profile contributes to their multiple therapeutic effects [6]. Hence, understanding the original properties of EOs is relevant to determine whether their biopharmaceutical properties remain intact during DDS preparation, while also aiming to reduce degradation and evaporation of volatile compounds, thus enhancing storage stability.

In this context, liposomes are considered among the safest DDS, due to their biocompatibility, low toxicity, and versatility in encapsulating both hydrophilic and lipophilic drugs. Moreover, they represent one of the most widely commercialized delivery platforms to date, with several liposomal formulations already approved for clinical use as antimicrobial and anticancer agents [7,8]. Liposomes are typically composed of either synthetic or naturally derived phospholipids, including lecithin which contributes to the formation of stable bilayer structures, while maintaining good biocompatibility and biodegradability [9]. Many drug delivery systems, such as bioactive liposomes, are usually prepared using high-energy methods, i.e., sonication [10], that could negatively affect the oil composition and overall stability structure of bioactive nanocarriers [2]. Recently, a potent inhibition effect against pathogenic bacteria within the biofilm has been reached by loading nutraceuticals and/or antimicrobial agents into bioactive liposomes [11]. Hence, successful nanocarrier preparation and characterization require a multidisciplinary approach, based on integrated insights from chemistry, physics and biology.

In the present paper, *Thymus vulgaris* essential oil (TEO) has been employed in the preparation of bioactive liposomes able to enhance TEO performance by protecting its mixture, which is intrinsically volatile, unstable, and cytotoxic [3,12–14]. In addition, resveratrol (RV), a natural polyphenol primarily found in grapes and berries and endowed with effective antimicrobial properties has been also incorporated into vesicular systems to overcome its low bioavailability and enhance effective pharmaceutical applications [15–17]. Resveratrol and thyme oil are both natural components known for their broad-spectrum antimicrobial activity. Resveratrol, a polyphenolic compound primarily found in grapes and berries, has been extensively studied for its antibacterial and antifungal properties [15,18]. Similarly, thyme oil, rich in bioactive constituents such as thymol and carvacrol, has demonstrated strong efficacy against a variety of microbial strains [19,20]. When used in combination, these two agents could exert complementary or even synergistic effects, potentially enhancing their mutual antimicrobial activity. This interaction opens new opportunities for the design of multifunctional delivery systems. In particular, the incorporation of thyme oil into a bioactive carrier could strengthen the overall antimicrobial potential of resveratrol, improving its efficacy, stability, and bioavailability. Such an approach may offer a promising strategy for the development of advanced antimicrobial formulations, especially in the context of increasing microbial resistance. Thus, exploring the co-delivery of these compounds within an engineered carrier system represents a valuable direction for future research. Moreover, the liposomal system was designed to protect and facilitate targeted delivery of RV and TEO directly to bacterial biofilms [11,21]. A comparison of the chemical profile of TEO as such, and in the loaded and empty formulations, has been carried out by applying a Headspace Solid Phase Microextraction/Gas Chromatography-Mass Spectrometry (HS-SPME/GC-MS) technique. SPME embodies a solvent-free technique satisfying most of the principles of green analytical chemistry [22] and it relies on a microextraction process not altering any feature of the sample [23]. Moreover, GC/MS analysis is recognized as the gold standard for chemical characterization of EOs whose (semi-)-volatile and volatile components can be easily separated, identified and quantified [24]. High-Performance Liquid Chromatography with Ultraviolet Detection (HPLC-UV) has been useful to determine stability and composition of TEO throughout the whole production process.

Thus, the two main isomeric metabolites, thymol and carvacrol, have been quantified in TEO, TEO after sonication (TEO-s), in empty (LT) and RV loaded (LT-RV) liposomes. The results provided a critical insight into whether the EO undergoes compositional changes during processing, to optimize the production process. The antimicrobial activity of the formulations was then tested, using as experimental model *Listeria* spp., Gram-positive rod-shaped bacteria that inhabit various environments. *Listeria monocytogenes* and *Listeria ivanovii* are the predominantly pathogenic species: while *L. ivanovii* most often causes infections in ruminants, *L. monocytogenes* primarily affects humans, causing listeriosis, a rare but serious and mainly food-borne infection [25]. Its environmental persistence, partially attributed to the ability to form biofilms, has been recognized to confer bacterial cell protection to antimicrobial compounds and stressful environments.

The European Centre for Disease Prevention and Control (ECDC) reported *L. monocytogenes* as a Public Health issue. In 2023, the European Union recorded the highest number ever of infections caused by Shiga toxin-producing *Escherichia coli* (STEC) and *L. monocytogenes* since the start of EU-wide epidemiological surveillance in 2007 [26,27]. Overall, this multidisciplinary study, including diverse scientific expertise and advanced analytical methodologies, has allowed to gather a thorough evaluation of the bioactive liposomal formulation, which ultimately proved to be microbiologically effective.

2. Materials and methods

2.1. Materials

Cholesterol (CHOL), pyrene, Hepes salt (N-(2-Hydroxyethyl)piperazine-N′-(2-ethanesulfonic acid) sodium salt), 1,6-diphenyl-1,3,5-hexatriene (DPH), *Thymus vulgaris* essential oil were purchased from Sigma-Aldrich (Milan, Italy). Resveratrol was purchased by Farmalabor Srl (Canosa di Puglia, Barletta, Italy). Soy lecithin (SL), Dialysis membranes (MWCO 8000 Da), ethanol, methanol and chloroform were provided from Carlo Erba Reagents Srl (Cornaredo, Milan, Italy). All other products and reagents were of analytical grade.

2.2. GC/MS analysis of TEO and TEO-s

To compare the chemical profile of TEO and TEO-s, GC/MS analyses were performed using a Clarus 500 model PerkinElmer (Waltham, MA, USA) gas chromatograph equipped with FID (flame detector ionization) and coupled with a single quadrupole mass spectrometer (Clarus 500 model PerkinElmer), was used to carry out the analyses. A capillary

column (Varian Factor Four VF-5; 60 m × 0.32 mm ID, DF = 1.0 μm) was housed in the GC oven whose programmed temperature was set initially at 40 °C then a gradient of 6 °C/min to 220 °C for 15 min. The injector GC was set at 270 °C. Helium was used as carrier gas at a constant rate of 1 mL/min. MS detection was performed with electron ionization (EI) at 70 eV operating in the full-scan acquisition mode in the *m/z* range 35–550 amu. To identify the volatile compounds, the MS-fragmentation pattern obtained was compared with those of pure components stored in the NIST11 mass spectra library database. Further, the Linear Retention Indices (LRIs) were calculated using a mixture of *n*-alkanes (C_8–C_{30} aliphatic hydrocarbons), injected under the same operating conditions. The relative amounts of the components were expressed as percent peak area relative to total peak area without the use of an internal standard and any factor correction. The analyses were carried out in triplicate.

2.3. Preparation of liposomes

LT and LT-RV were prepared using the thin-layer evaporation technique [28]. The sample composition is reported in Table 1. Briefly, SL and CHOL were dissolved in a mixture of chloroform and methanol (3:1 v/v). The solvent was removed using a rotary vacuum evaporator for 1 h at room temperature (Rotavapor® R-210, Büchi-Italia S.r.l., Assago, Milan, Italy). To ensure complete organic solvent evaporation, the sample was kept for another hour in a T51 glass oven dryer (Büchi-Italia S.r.l., Assago, Milan, Italy). For RV-loaded liposomes, RV was dissolved with the lipids due to its lipophilic nature. The lipid film was hydrated with Hepes buffer (10 mM, pH 7.4) and to remove the film from the tube walls, the sample was stirred by using a vortex mixer. After multilamellar liposome formation, TEO was added. In order to obtain unilamellar vesicles, the samples were sonicated with a 20 % of amplitude, at 4 °C, for 4 min, with a pulse on 1sec and pulse off 1 s by using a microprobe operating at 20 kHz (VibraCell-VCX 600-Sonics- Taunton, MA, USA) under continuous nitrogen flow in order to limit lipid and EO chemical degradation.

To obtain a monodisperse sample, the larger vesicles were removed by centrifugation at 10.000 rpm and 10 °C for 10 min (MPW-260R). Afterwards, the supernatant was ultracentrifuged (30.000 rpm and 10 °C for 6 h) to remove the unencapsulated RV and TEO. Finally, the pellet was resuspended in the same volume of Hepes buffer.

2.4. HD, ζ-potential, PDI and RV EE %

All samples were analyzed using a Dynamic light scattering, DLS (Zetasizer Nano ZS 90, Malvern, UK) with a scattering angle of 90.0°and equipped of a 5 mW HeNe laser ($\lambda = 632.8$ nm) to determine the particle size and electrophoretic mobility. The cumulant method was employed to calculate the HD and the polydispersity index (PDI) [29]. The electrophoretic mobility (μ) was converted into ζ-potential using the Smoluchowski relation $\zeta = \mu\,\eta/\varepsilon$, where η and ε represent the viscosity and the permittivity of the solvent phase, respectively [30].

The determination of the RV content was measured by UV–visible spectroscopy (PerkinElmer, Lambda 3a) to evaluate the amount of RV entrapped into liposomes. Initially, a calibration curve of RV was constructed by measuring the UV absorbance at 306 nm of a series of known RV concentrations. The analytical curve was obtained by testing several RV concentrations and showed a linear correlation of 0.9985. The equation used to calculate the RV concentration in the samples was: y = 31.317x - 0.0222. This calibration curve was subsequently used to quantify the RV content in the liposomal formulation (LT-RV).

Table 1
Samples composition of LT and LT-RV.

Sample	SL (mg/mL)	CHOL (mg/mL)	TEO (mg/mL)	RV (mg/mL)
LT	10	5.8	6	–
LT-RV	10	5.8	6	1

The encapsulation efficiency (E.E. %) was calculated as:

$$EE\,\% = \frac{Entrapped\ drug\ (mg)}{total\ drug\ used\ (mg)}\ x\ 100$$

2.5. Fourier-transform infrared spectroscopy (FT-IR)

Fourier-transform infrared spectroscopy (FT-IR) has been widely applied to determine subtle alternation of chemical structure of liposomes. FTIR was performed on a Spectrum Two FTIR spectrometer (PerkinElmer) equipped with a Universal ATR accessory. 10 μL of each sample were added to the ATR crystal and allowed to completely dry before the measurement. The lever was used to ensure good contact with the crystal. The spectra were obtained using software Spectrum (version 6.2.0), a Spectral resolution of 4 cm^{-1}, a range of 4000–450 cm^{-1} and 32 scans per sample.

2.6. Morphological analysis: transmission electron microscopy

Transmission electron microscopy was used to visualize morphological aspects of empty and RV-loaded liposomes. 10 μL of liposome samples were put onto a 400 mesh TEM carbon-coated copper grid and counterstained by a drop of an aqueous solution of 2 % (v/v) phosphotunstic acid (PTA) (pH 7.0). After removing the excess of stain by an absorbent pad, samples were imaged under a FEI 280S transmission electron microscope (FEI Company, Hillsboro, OR, USA) at an acceleration voltage of 100 kV. Images were processed with Adobe Photoshop CS4 software (Adobe Systems, San Jose, CA, USA) for editing.

2.7. Fluorescent anisotropy spectroscopy

DPH is a fluorescent probe commonly used to monitor the anisotropy (correlated with the fluidity) of lipophilic membranes [31]. DPH is known to localize into the hydrophobic region of the bilayer; this makes it useful for characterizing the region and assessing the effect of RV trapping [32]. DPH molecules are often aligned in parallel arrangements in the hydrophobic part of the phospholipid bilayer. Its anisotropy is related to the rotational diffusion motion of the probe throughout the bilayer. It is highly sensitive to the order of lipid chains and membrane fluidity [33]. The anisotropy values reflect the degree of symmetry and fluidity of lipid membrane. DPH-loaded liposomes were prepared by co-dissolving lipids and the probe (2×10^{-3} M) in a mixture of organic solvents [28].

The fluorescence anisotropy (*A*) was determined using the following formula:

$$A = \frac{(I_{VV} - I_{VH}) \times G}{(I_{VV} + 2I_{VH}) \times G}$$

where I_{VV}, I_{VH}, I_{HV} and I_{HH} are the intensities ($\lambda_{exc} = 350$ nm, $\lambda_{em} = 428$ nm) of the fluorescence measured using a LS5013 PerkinElmer spectrophotometer, with *V* (vertical) and *H* (horizontal) orientation of the polarized light. The *G* factor is defined as $G = I_{HV}/I_{HH}$, the ratio of sensitivity of the detection system. Anisotropy provides information about the rotational mobility of the fluorescent probe, revealing information about membrane fluidity, lipid packing, and interactions with other molecules.

2.8. Polarity and microviscosity evaluation

Pyrene is a hydrophobic probe used to investigate the microviscosity and micropolarity of vesicle bilayer. The probe (1 mM) was incorporated into liposomes along with the lipids. Fluorescence emission spectra were collected from 350 to 550 nm at a λ excitation of 330 nm. The polarity of the environment was assessed by calculating the ratio of the first (I_1) and the third (I_3) vibrational peaks in the emission spectra, as these peaks are sensitive to changes in the surrounding medium's polarity [34].

Conversely, the microviscosity was determined by the ratio of the excimer emission intensity (I_E) to the third vibration band (I_3).

2.9. HPLC-UV experiments

Samples of the TEO for HPLC-UV experiments were prepared by diluting TEO and sonicated TEO (TEO-s) in a 50:50 mixture of water and acetonitrile. LT and LT-RV were broken before analysis by diluting the suspension of either liposome in Hepes with a 10-fold higher volume of DMSO.

HPLC experiments were performed using a Thermo Vanquish system (Thermo Fischer) equipped with a vacuum degasser, quaternary solvent mixer, and a diode array detector (DAD). UV spectra were collected across the range of 200–900 nm, with chromatograms extracted at 270–278 nm. The Xcalibur software was used for instrument control, data collection, and data processing. The column used was a XTerra C18 (4.6 × 250 mm, 5 μm). An isocratic elution with a 50:50 mixture of acetonitrile and water (CH_3CN:H_2O) was employed at a flow rate of 1 mL/min, following an analytical method described in the literature [35]. The injection volume for all samples and standard solutions was 20 μL.

Linearity was tested by comparing the relationship between the concentration of thymol and carvacrol standards with the obtained absorbance, yielding determination coefficients (r^2) > 0.997.

2.10. Stability studies

2.10.1. HS-SPME-GC/MS analysis of LT and LT-RV

The extraction of the volatile components from LT and LT-RV was achieved by means of SPME technique followed by GC/MS analysis. Each sample (ca. 2 mL) was placed individually inside a 7 mL glass vial with PTFE-coated silicone septum and a SPME device from Supelco (Bellefonte, PA) with 1 cm fiber coated with 50/30 μm DVB/CAR/PDMS (divinylbenzene/carboxen/polydimethylsiloxane), was used to adsorb the volatiles. After conditioning the fiber, it was exposed to the headspace of the sample for 2 min at 30 °C. Then, for the desorption of the components, the fiber was inserted in the GC injector maintained at 250 °C in spitless mode. Before moving on to the next sample, the fiber was reconditioned.

For the GC-MS analysis the same apparatus described in Section 2.2, was used. In this case, the injector GC was set at 250 °C while the applied temperature program was the same. The identification and quantification of the components were performed as reported in the previous Section 2.2. The analyses were conducted in triplicate.

2.10.2. Assessment of liposomal stability over time: DLS analysis

The stability of the suspensions was assessed by measuring the hydrodynamic diameter (HD) and ζ-potential of LT and LT -RV at various intervals after preparation: daily for the first week and then weekly for samples stored at room temperature and 4 °C. The sample was appropriately diluted using the same buffer as used for the preparation. Size and ζ-potential measurements were performed on at least three different sample preparations for each sample. Results are reported as the average value ± standard deviation.

2.10.3. Stability of free and liposome-entrapped RV: UV–Vis spectrophotometer analysis

UV–Vis spectroscopy was employed to evaluate the stability of free and entrapped RV at room temperature and 4 °C for a period of 3 months.

As explained above, the determination was carried out using the calibration curve at different time intervals (1, 30, 60, and 90 days).

2.10.4. Evaluation of vesicle stability in culture media: DLS and UV–Vis spectrophotometer analyses

The vesicle stability in different media was monitored in terms of size using DLS and RV release, using UV–Vis spectroscopy, following the same conditions as the microbiological studies.

Precisely, stability studies of both empty and RV loaded liposomes were conducted over a 72-h period in the DMEM, FBS, TBS and BHI culture media.

A volume of 100 μL of sample was mixed with 900 μL of medium, to achieve the minimum optimal dilution for properly observing the sample using DLS, and subjected to magnetic agitation at a controlled temperature of 37 °C. The size and ζ-potential of each sample, in contact with each medium, were analyzed hourly for the first 8 h, and then at the 24th, 48th, and 72nd hours.

The experiment was carried out over a 72-h period at 37 °C to simulate the experimental conditions of microbiological studies and to monitor changes in terms of size and PDI of the samples. When introduced into complex biological media containing electrolytes, proteins, lipids, *etc.*, liposomes are subjected to a range of forces that influence their behavior. These interactions can significantly affect their stability, as well as their ultimate fate [36].

In-vitro drug release was investigated by using a cellulose acetate membrane (MWCO 8 kDa, Spectra/Por®, Rancho Dominguez, CA, USA), in DMEM, FBS, TBS and BHI culture medium at 37 °C, to monitor RV release in an environment that simulates microbiological experimental conditions for 72. To determine the amount of RV released, and indirectly the stability of the vesicles, 1 mL aliquots were withdrawn from the release medium every hour, and the absorbance was measured by UV analysis as described above. Then, the aliquots were re-inserted into the external medium. Analysis was performed immediately after each sampling.

2.11. RV release study in Hepes buffer: UV–Vis spectrophotometer analyses

The release experiment, conducted by using a cellulose acetate membrane, was performed to monitor the release of RV in Hepes buffer, pH 7.4, over time. The experiment was carried out for 24 h at 37 °C using the same methodology explained in the previous section.

2.12. Bacterial strains

Listeria spp. strains of different origins were used. As reference strains, *L. ivanovii* ATCC 19119 and *L. innocua* ATCC 1172 (ATCC, Manassas, USA) were tested. *L. monocytogenes* LM2 and LM9, both of clinical origin and belonging to serotype 1 and 4, respectively, were obtained from a laboratory collection of the Department of Public Health and Infectious Diseases, "Sapienza" University of Rome [37]. Strains, isolated on Oxford agar, were grown overnight at 37 °C in Brain Heart Infusion Broth (BHI, Oxoid, Basingstoke, UK) and stored at −80 °C in glycerol.

2.13. Determination of minimum inhibitory concentration (MIC) and minimum Bactericidal concentration (MBC)

The MIC determination of the substances was performed by the microdilution method. 10 μL of exponentially growing bacterial cultures diluted to 0.5 McFarland were added to 190 μL of BHI (Oxoid Ltd., Basingstoke, UK) containing the preparations at concentrations ranging from 130 μg/mL to 4 μg/mL. After the incubation at 37 °C for 24 h, the MIC was considered as the lowest concentration at which no visible growth is observed. MBC was determined, by sub-culturing on Tryptic Soy Agar (TSA, Oxoid, Basingstoke, UK) for 24 h, 10 μL from each well with no visible growth. MBC is defined as the lowest drug concentration that kills 99.9 % or more of the bacterial inoculum.

2.14. Biofilm formation

Listeria spp. strains were tested for their ability to form biofilms, according to the model described by Stepanović et al., [38]. The strains

were cultured on Tryptone Soy Broth (TSB, Oxoid, Basingstoke, UK) supplemented with 0.6 % yeast extract, and the microorganisms were incubated at 37 °C for 16–18 h. The bacterial suspensions, at a concentration of 10^6 CFU/mL, were inoculated into 96-well microplates. The plates were then incubated for 24 h at 37 °C. After 24 h, the wells were washed three times with phosphate-buffered saline (PBS 1X, Sigma-Aldrich; Milan, Italy). The plates were then dried and fixed using 99.9 % methanol and subsequently stained by adding 150 μL of a 2 % (v/v) crystal violet solution to each well for 15 min. Excess dye was removed by washing with water. Finally, the crystal violet was solubilized by adding 150 μL of 96 % (v/v) ethanol to each well for 30 min at room temperature. The absorbance was measured at 570 nm using a microplate reader (Bio-Rad Benchmark, USA). The interpretation of the data was based on a cut-off value, which allowed the classification of the tested strains as non-biofilm producers, weak, moderate, or strong biofilm producers [39].

The OD cut-off was calculated as the mean OD of the negative control (NC) plus three times its standard deviation (SD).

The results were then interpreted as follows.

- OD ≤ OD cut-off: non-biofilm producer
- OD cut-off ≤ OD ≤ 2x OD cut-off: weak biofilm producer
- 2x OD cut-off ≤ OD ≤ 4x OD cut-off: moderate biofilm producer
- OD ≥ 4x OD cut-off: strong biofilm producer

2.15. Effect of LT and LT-RV on bacterial biofilm production

In order to evaluate the biofilm inhibition induced by the different substances, 20 μL of each bacterial strain (1–2 × 10^8 CFU/mL) was inoculated into wells of a 96 well plate containing 180 μL of TSB supplemented with these substances at a sub-MIC concentration (10 and 5 μg/mL for all the substances with the exception of the oil, tested at 4 and 2 μg/mL). The inhibition of cell attachment was evaluated after 24 h of incubation with the substances. The plates were stained with crystal violet and treated as described above. The absorbance was measured at 570 nm using a microplate reader (Bio-Rad Benchmark, USA. The percentage of biofilm inhibition by the preparations has been calculated using the following formula:

$$Biofilm\ inhibition\ (\%) = 100 - (OD570\ sample\ /\ OD570\ control \times 100)$$

Values higher than 40 % were considered relevant in biofilm inhibition.

2.16. Effect of LT and LT-RV on bacterial biofilm eradication

The impact of the substances on pre-formed biofilms was assessed after an initial 24 h of bacterial growth period in polystyrene 96-well plates at 37 °C. Following this incubation, the supernatant was aspirated, and the wells were replenished with fresh medium containing the preparations at sub-inhibitory concentrations (10 and 5 μg/mL for all the substances except for the oil, tested at 4 and 2 μg/mL). The plates were then incubated at 37 °C for an additional 24 h with the treatment. After incubation, unattached bacterial cells were removed by aspiration. The biofilms were then washed twice with PBS 1X and then stained with 2 % crystal violet solution for 20 min, as previously described. The crystal violet was solubilized with 95 % ethanol, and the absorbance was measured at 570 nm using a microplate reader (Bio-Rad Benchmark, USA). The percentage of biofilm eradication has been calculated with the same formula used for inhibition. Formulations with a percentage value higher than 40 % were considered capable of eradicating the biofilm.

2.17. Scanning electron microscope (SEM) analysis

Biofilm samples were prepared following previously reported protocols [40,41]. Briefly, bacterial biofilms were grown on aluminum stubs and subsequently fixed in a solution of 2.5 % glutaraldehyde prepared in 0.1 M phosphate buffer (PB), pH 7.4. After 48 h of fixation, samples were washed twice in a phosphate buffer for 10 min each. For post-fixation, specimens were incubated in 1 % osmium tetroxide (OsO_4) in distilled water for 1 h to enhance membrane contrast and electron density. Following this step, samples underwent two sequential washes in distilled water before being immersed in a 1 % tannic acid solution (prepared in distilled water) for 30 min. A final wash in distilled water was performed prior to imaging. Samples were examined using a Hitachi SU3500 SEM operating under high vacuum conditions with an acceleration voltage of 7 kV. The incorporation of tannic acid (impregnation procedure) following osmium post-fixation enhanced structural stability, preventing beam-induced damage and ensuring high-resolution imaging, even under high vacuum. Notably, the omission of conventional dehydration steps preserved the biofilm architecture in its fully hydrated state, minimizing structural artifacts. This approach allowed for high-magnification imaging, revealing the ultrastructural integrity of *Listeria* cells with exceptional clarity.

2.18. Statistical analysis

All experiments were repeated three times (n = 3). Data are presented as mean ± SD. Statistical analysis was performed using GraphPad Prism 10 (one-way ANOVA with Tukey's multiple comparisons test; $p < 0.05$ considered significant).

3. Results and discussion

3.1. Chemical composition of TEO and TEO-s

The GC-MS of the essential oil (TEO) and the sonicated one (TEO-s)) highlighted an almost superimposable chromatographic profile. No qualitative difference was observed. From a quantitative point of view Table 2 shows that the average percentage values of the compounds follow the same trend respecting the identical order of magnitude.

Table 2
Chemical composition (percentages mean values ± standard deviation) of TEO and TEO-s.

N°	Component[a]	LRI[b]	LRI[c]	TEO	TEO-s
1	*α*-pinene	930	932	3.6 ± 0.05	2.0 ± 0.02
2	camphene	942	946	1.1 ± 0.04	0.7 ± 0.04
3	*β*-myrcene	981	987	1.5 ± 0.05	1.2 ± 0.05
4	*p*-cymene	1022	1026	22.7 ± 1.20	19.8 ± 1.15
6	1,8-cineole	1030	1033	1.4 ± 0.06	1.7 ± 0.10
5	*γ*-terpinene	1058	1062	6.6 ± 0.15	4.7 ± 0.06
7	linalool	1091	1095	6.5 ± 0.18	7.9 ± 0.08
8	*α*-campholenal	1128	1132	0.1 ± 0.01	0.1 ± 0.01
9	camphor	1132	1139	1.1 ± 0.05	1.2 ± 0.05
10	isoborneol	1148	1153	0.3 ± 0.02	0.3 ± 0.02
11	endoborneol	1155	1160	0.2 ± 0.02	0.3 ± 0.02
12	terpinen-4-ol	1183	1182	1.8 ± 0.06	2.2 ± 0.06
13	thymol	1270	1272	43.0 ± 4.02	49.1 ± 5.15
14	carvacrol	1395	1397	8.2 ± 0.10	6.4 ± 0.12
15	*β*-caryophyllene	1437	1440	0.5 ± 0.03	0.3 ± 0.02
16	caryophyllene oxide	1575	1580	1.3 ± 0.07	2.0 ± 0.06
17	humulene epoxide II	1610	1608	0.1 ± 0.01	0.1 ± 0.01
	SUM			100.0	100.0
	Monoterpenes			96.9	96.3
	Sesquiterpenes			1.9	2.4
	Others			1.2	1.3

[a] The components are reported according to their elution order on apolar column.
[b] Linear Retention indices measured on apolar column.
[c] Linear Retention indices from literature; tr: traces (mean value < 0.1 %).

3.2. Size and morphological analysis

Preliminary formulative studies were carried out to identify the optimal formulation in terms of composition. The surfactant concentration was set to assure the bilayer formation [34]. Moreover, the aim was to obtain the highest possible amount of RV and oils while ensuring proper vesicle formation and a homogeneous suspension. Moreover, the effect of varying CHOL content with respect to oil amount, was evaluated. The sample prepared with an intermediate CHOL concentration was selected, as it provided a bilayer with intermediate rigidity (anisotropy, see Table S2) neither too fluid, which could compromise stability, nor excessively rigid, which could hinder the release of the encapsulated compound. After confirming that the composition of the EO was not significantly or qualitatively altered by the sonication conditions applied for liposome preparation, the sample was subjected to characterization. Specifically, HD, polydispersity index (PDI), and ζ-potential were measured, with the results presented in Table 3. These features are essential to define the physicochemical profile of the formulations and to determine their suitability for antimicrobial application. In particular, features such as size distribution and surface charge influence the system stability, the release dynamics of encapsulated compounds, and the interactions with biological targets such as membranes, cells, and bacteria. Moreover, the evaluation of these parameters also provides indirect validation of the preparation method employed. Techniques such as sonication, whose operational parameters (e.g., time, amplitude, cycles, and temperature) can be finely tuned, enable the modulation of vesicle characteristics according to the desired application. Consequently, the ability to control and reproducibly obtain specific colloidal properties is essential not only for ensuring functionality but also for optimizing and standardizing the preparation process.

DLS analyses show that both empty and loaded liposomes appear similar in terms of hydrodynamic diameter (HD), PDI, ζ-potential. They have a HD around 180 nm and the PDI values are lower than 0.20, indicating that LT and LT-RV are characterized by a monodisperse liposome population [42,43]. Notably, the size of RV-loaded and empty liposomes falls within the same range, a crucial feature to ensure comparable *in vitro* and *in vivo* behavior of the carriers, as liposome size significantly influences cell internalization, interaction with membranes or bacteria, and consequently impacts their efficacy and potential toxicity [44].

The ζ-potential is highly negative for both samples (≅ -50 mV) due to the presence of SL, a value more negative than −30 mV that is typically associated with good stability over time, as it ensures strong repulsive forces between the vesicles. SL is a mixture of phospholipids with a predominance of phosphatidylcholine, which has a neutral charge. However, it also contains phosphatidylserine and phosphatidylinositol, which can impart a significant negative charge to the liposomal surface [44,45]. Also, the presence of RV did not significantly affect the surface charge of the samples, suggesting that this natural compound is likely entrapped in the liposomes [46].

Morphological analysis performed by TEM (Fig. 1) showed that both LT (Panels a and b) and LT-RV vesicles (Panels c and d) appear almost spherical in shape and partially deformed with the typical cup shape. The dimensions correspond with good approximations to DLS measurements. At higher magnification (b and d) the liposomes appear as multilayered vesicles with well-defined layers. The incorporation of RV does not compromise the layered structure but only causes a slight reduction in size. Despite the possibility of modifying the sonication parameters to further influence the morphology of the liposomes to obtain unilamellar vesicles, the formulation strategy prioritized preserving the oil composition. Accordingly, a compromise was reached by retaining the existing sonication conditions, which still allowed for the formation of multilamellar liposomes exhibiting appropriate size and low polydispersity index (PDI) [28].

3.3. LT-RV EE % evaluation and FTIR analysis

The content of RV in liposome formulations was quantified by UV–Vis spectrophotometry.

The EE% of RV was approximately 25 %. These results suggest that a significant amount of RV was lost during the purification process. As reported by B.D. Isailović et al., high shear forces during sonication can disrupt liposomal structures, leading to leakage of RV [46]. Moreover, the incorporation of TEO into the lipid bilayer likely affects the spatial organization of the vesicle structure, potentially impacting the final EE% of RV [47]. Nevertheless, the amount of entrapped RV may be still sufficient to exert its antibacterial activity against *Listeria* spp. and other bacterial pathogens [18].

Different strategies could be employed to assess the interaction and internalization of resveratrol (RV) within the nanocarriers, such as Differential Scanning Calorimetry (DSC) and Fourier-Transform Infrared Spectroscopy (FTIR) [48]. In this study, FTIR analyses were performed. FT-IR was applied to investigate the vibrational features of three samples, LT, LT-RV and RV alone, with the aim of assigning changes in the wavenumber of specific absorptions to interaction occurring between the functional groups of liposomal bilayer components.

The FTIR spectra (Fig. 2) of the three samples (LT in black, LT-RV in red and RV in blue) show distinct spectral features that reflect their chemical composition.

The RV spectrum exhibits characteristic peaks in the aromatic region, particularly at 1605 cm^{-1} and 1585 cm^{-1}, attributed to C=C stretching vibrations of aromatic rings, and a broad OH stretching band around 3210 cm^{-1}, typical of phenolic groups involved in strong H-bonds. C-O stretching vibrations appear in the fingerprint region at 1324 cm^{-1}, 1234 cm^{-1}, 1035 cm^{-1}, and 804 cm^{-1} [49].

In the case of LT, the spectrum is dominated by a pair of intense peaks in the 2800-3000 cm^{-1} range, representing, according to literature, the aliphatic C-H stretching bands, typical of the lipid chains of CHOL and lecithin [50,51]. Contribution may also arise from thymol, the most abundant component of TEO, which shows three relevant absorptions in the same spectral range [52]. The broad band at 3400 cm^{-1} is attributable to OH stretchings involved in H-bonds and is consistent with spectra reported in the literature for lecithin, CHOL and thymol. A distinct ester carbonyl peak appears at 1738 cm^{-1}, while phosphate-related bands are observed around 1231 cm^{-1} and 1076 cm^{-1}, confirming the presence of phospholipids.

The LT-RV spectrum, retains the lipid-associated features of LT, including the C-H stretching bands (2854 cm^{-1}, 2928 cm^{-1}) and the ester carbonyl at 1738 cm^{-1}, but also displays enhanced intensity in the aromatic region, notably at 1586 cm^{-1}, confirming the presence of RV. The intensity increase of the band at 3400 cm^{-1}, together with the absence of the 3210 cm^{-1} band present in the RV spectrum, suggests that the strong H-bonds which are formed between RV hydroxyl groups in the pure compound are disrupted upon interaction with the liposome bilayer. This evidence indicates weaker hydrogen bonds with the phospholipids are formed, suggesting that RV interacts with liposome structure [52,53] in agreement with anisotropy fluorescence results.

Table 3
HD, PDI, ζ-Potential, EE%, polarity (A.U), microviscosity (A.U), and anisotropy (A.U), values of samples.

Sample	HD ± SD (nm)	PDI ± SD	ζ-potential ± SD (mV)	EE_{RV} (%)	I_1/I_3 (polarity)	I_E/I_3 (micro-viscosity)	Anisotropy (fluidity)
LT	181 ± 8	0.18 ± 0.01	−51 ± 3	–	1.24 ± 0.02	0.58 ± 0.02	0.29 ± 0.01
LT-RV	176 ± 2	0.18 ± 0.01	−47 ± 4	24 ± 2	1.26 ± 0.01	0.51 ± 0.01	0.33 ± 0.01

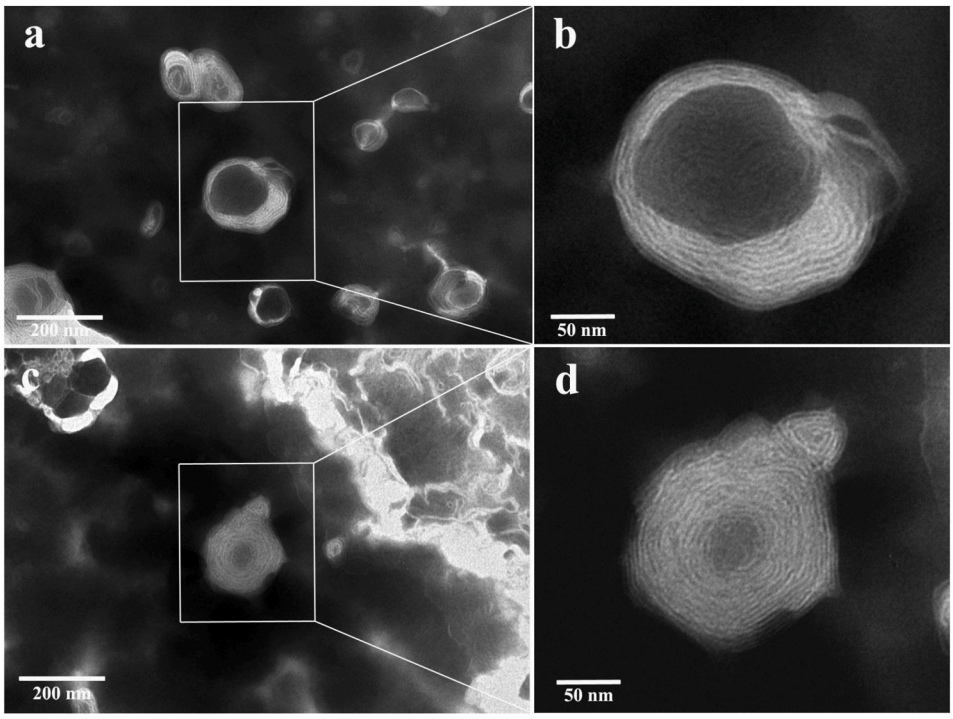

Fig. 1. TEM representative images of LT (Panels a and b) and LT-RV (Panels c and d) under negative staining.

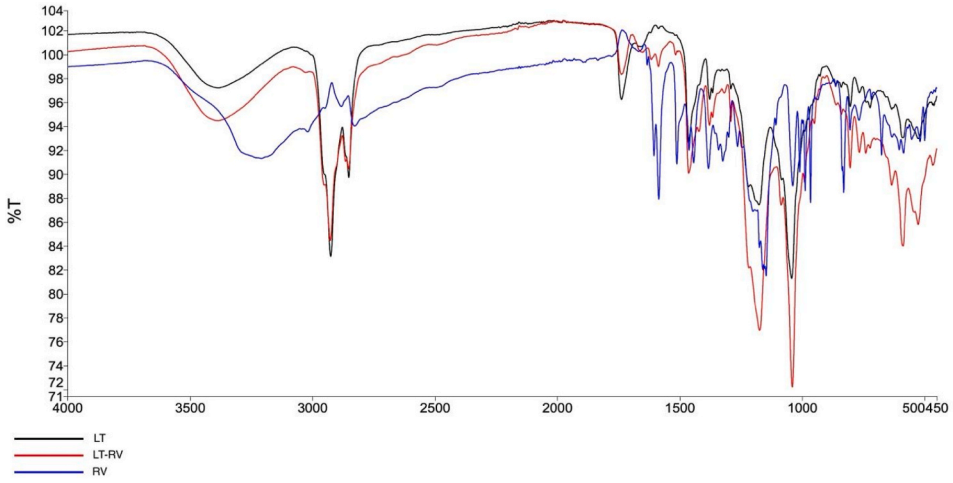

Fig. 2. FTIR spectra of LT, LT-RV and free RV.

3.4. *Polarity, microviscosity and fluidity: fluorescence studies*

To assess bilayer properties such as polarity, microviscosity, and fluidity, two hydrophobic fluorescent probes—DPH and pyrene—were employed (Table 3).

The comparison of polarity (I_1/I_3), microviscosity (I_E/I_3), and anisotropy (fluidity) between LT and LT-RV reveals some slight differences, although the values remain largely within the same range. This suggests that the inclusion of RV into the structure does not significantly affect the bilayer features. These findings are consistent with the DLS data, which show no appreciable differences in size, ζ-potential, or PDI between the empty and RV-loaded formulations. In particular, pyrene is sensitive to changes in polarity of the microenvironment, as reflected in the magnitude of the I_1/I_3 ratio. Additionally, the fluorescent nature of pyrene can reflect the degree of molecular ordering of the membrane [54]. Generally, a lower I_1/I_3 value indicates a lower membrane micropolarity and a smaller proportion of hydrophilic structures on the membrane. Comparing the polarity values of LT and LT-RV, the slight increase is not significant. Pyrene is also a useful probe for assessing membrane fluidity, as it forms excimers depending on the extent of molecular mobility within the bilayer. This parameter is sensitive to the presence of additives such as CHOL or RV, which can significantly modulate bilayer dynamics and, consequently, excimer formation [55]. The pyrene molecule is located in the inner region of the membrane and the excimer is formed by bifluorophore molecules, and information about "microfluidity" is obtained by relating I_E and I_3 [56]: the higher the I_E/I_M ratio, the more fluid the membrane [47–49]. Indeed, for both samples, a low excimer is formed (Fig. S1), which demonstrates low probe mobility and a low tendency to form dimers, thus could suggest, according with the anisotropy data, that the probe is solubilized in a structurally rigid and ordered vesicle environment.

The obtained anisotropy values (higher anisotropy value near 0.4 A

U. is correlated with increased membrane rigidity) [57] indicate a comparable degree of rigidity in both the RV-loaded and empty liposomes, implying that the observed structural rigidity is an intrinsic property of the vesicle matrix itself, likely due to the presence of lecithin. Lecithin is known to promote the formation of tightly packed, less fluid bilayers, which can account for the restricted probe mobility and overall reduced membrane dynamics observed.

The inclusion of RV into liposomes shows a slight increase in the value, indicating a stiffening of the bilayer due to the incorporation of the lipophilic molecule. This effect is likely due to the hydrophobic interaction between bulky side chains of CHOL, the acyl chains of phospholipids and the RV [50].

3.5. Thymol and carvacrol quantification: HPLC-UV analysis

HPLC-UV analysis was performed to quantify the thymol and carvacrol isomers in TEO, TEO after sonication (TEO-s), and in the final formulations LT and LT-RV. Thymol, the most abundant component of the EO, was measured to determine the stability and entrapment efficiency (EE) of the EO during the formulation process, while carvacrol was quantified as a comparative marker to evaluate potential compositional changes. Separation of the standard samples of thymol and carvacrol showed good selectivity, as reported in the literature [35]. A standard chromatogram is reported in Fig. S2. The absorbance of samples diluted to concentrations ranging from 0.7 to 3.0 ppm was compared to calibration curves obtained by solubilizing the standards in a solution of Hepes and DMSO, as employed for the preparation and subsequent dissolution of the liposomes and finally diluting in water/-acetonitrile 50:50. The calibration curves and their corresponding equations are reported in Fig. S3.

Fig. 3 presents the quantities of thymol and carvacrol in TEO and TEO-s as % w/w of the two compounds relative to the initial quantity of TEO. Results show that in TEO approximately 84 % of the sample weight is composed of thymol, while carvacrol is present only in a lesser amount (3.5 % w/w). After sonication, the concentration of both thymol and carvacrol undergoes a significant decrease.

Results indicate that thymol, the principal component of TEO, is partially lost or degraded during sonication, therefore the reduced concentration observed will be used to determine the EE% of the oil in the liposomal formulation. The relative reduction of thymol and carvacrol concentrations after sonication of the sample appears to be the same (ca. 17 %) suggesting that the process has a limited impact on the overall oil composition.

When formulated into LT, the percentage of thymol and carvacrol incorporated into the formulation decreases to 24.6 % and 1.4 %, respectively, as reported in Table S3. These values were calculated by dividing the concentration of the two compounds (in μg/mL) by the initial concentration of TEO used for preparation. These results confirm that a significant portion of the oil is retained in the liposomes. The percentages of thymol and carvacrol in LT-RV are slightly higher than in LT, suggesting a potential stabilizing effect of RV on the liposome composition. Table S3 reports the exact concentrations. Based on these findings, the EE of TEO in the liposomal formulation was inferred. Specifically, the concentration of the most abundant component, thymol, was used. Fig. 4 reports the EE for LT and LT-RV, corresponding to 35 % and 41 %, respectively, indicating a higher retention of TEO in the presence of RV. Considering that a fraction of the liposomes is lost during the purification process, it can be inferred that most of the EO is effectively entrapped in the phospholipid bilayer. The observed reduction in the total thymol content is therefore likely attributable to the removal of the high-al low-density liposome fractions after centrifugation.

As a side note, the ratio between the two isomers remains rather constant across all samples, indicating no preferential integration of either isomer into the liposomal structure.

3.6. Stability studies over time: DLS analysis and UV–Vis spectrophotometry

Fig. 5 shows the stability of the liposomes over time, in terms of HD (panel A and C), ζ-potential (panel B and D) variation and RV EE%, monitored for 3 months at room temperature and 4 °C. For what concern the dimensions, both formulations show a similar trend, in particular LT shows a slight and gradual increase in size over 3 months. In contrast, LT-RV remains more stable throughout the entire duration of the experiment at both temperatures. This increased stability is likely due to the inclusion of RV within the liposomal structure, which, according to anisotropy values, appears to confer enough rigidity to the liposomes, and consequently, enhanced resistance over time [58]. In conclusion, both samples can be considered stable at both temperatures, as the variation is not significant.

The ζ-potential in all samples is strongly stable for up to 30 days, followed by a slight decrease between days 30 and 60, after which it reaches a new equilibrium. This phenomenon can be explained by several factors. SL is a complex mixture of various phospholipids that can rearrange within the liposomal membrane over time leading to changes in surface charge density and a reduction in the overall negative charge [59]. Additionally, the hydrolysis of phospholipids within the liposomes can form smaller molecules, such as free fatty acids, which alter the charge distribution on the membrane, resulting in a less negative ζ-potential [60].

The concentration of both free and encapsulated RV in liposomes was monitored over three-months at room temperature and at 4 °C. As shown in Fig. 5 (panels E and F), in both conditions the RV concentration exhibited only minimal progressive decreases. These results indicate that RV is stable both in solution and when encapsulated in liposomes, suggesting that the liposomal structural components do not negatively affect RV stability.

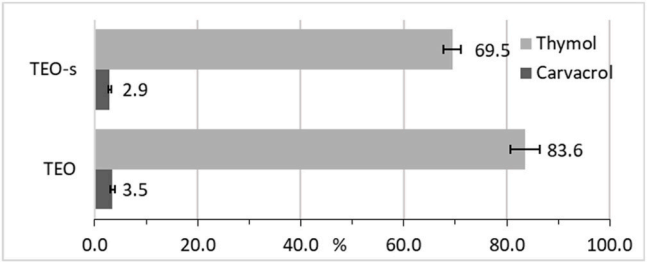

Fig. 3. Concentrations of thymol and carvacrol as % w/w compared to the initial concentration of TEO. Error bars represent standard deviation. Both carvacrol and thymol show statistically significant differences between the two groups ($p < 0.005$).

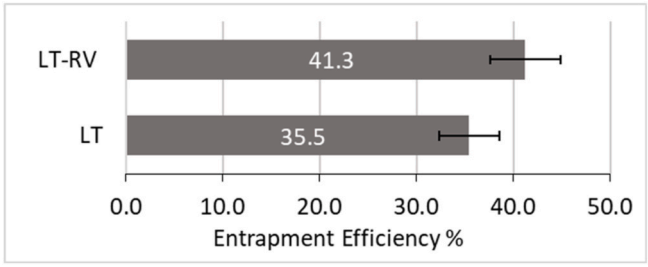

Fig. 4. TEO EE% in LT and LT-RV. Error bars represent standard deviation. Statistical significance of the data is confirmed by a p-value <0.05.

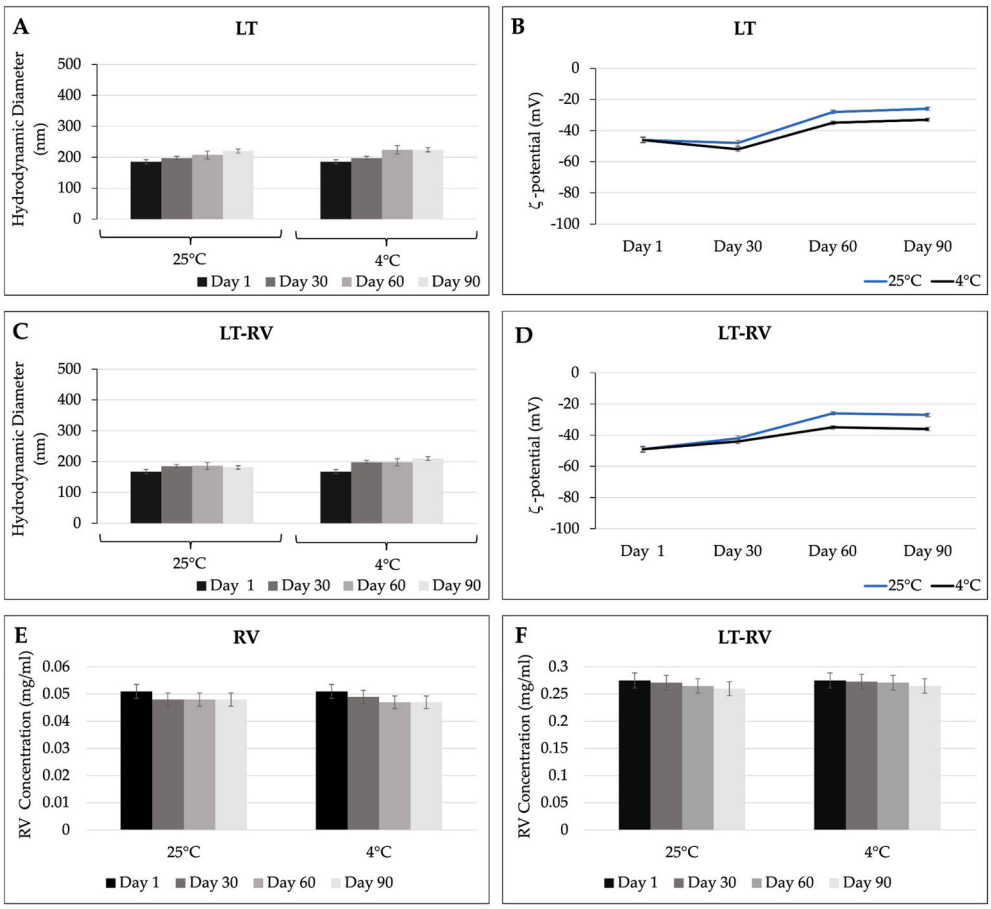

Fig. 5. Stability studies conducted using DLS to monitor the HD (panel A and C) and ζ-potential (panel B and D) over time, and using UV–Vis spectrophotometry to monitor free and loaded RV (panel E and F). The stabilities were carried out for 3 months at room temperature and 4 °C.

3.7. Volatile chemical composition of LT and LT-RV: HS-SPME-GC/MS analysis

By means of HS-SPME-GC/MS analysis, seventeen components were detected and identified. The monoterpene content is clearly higher than the sesquiterpene content, with thymol as the main component followed by *p*-cymene, *γ*-terpinene and carvacrol.

The analyses conducted revealed that the composition of LT (stored at 25 °C) remained almost stable over time. The only compound that undergoes a slight semi-quantitative variation is carvacrol. In fact, from Fig. 6, where the percentage values of the main compounds have been reported, it is possible to observe how the relative quantity of carvacrol increases during the first time interval (from day 0 to day 30) and then remains almost constant.

As for LT (stored at 4 °C), the data reported in Table S4 and in Fig. 7 show that the relative quantities of thymol and carvacrol increase at the expense of more volatile compounds, such as *p*-cymene and *γ*-terpinene.

In Tables S6 and S7 the chemical compositional profiles of LT-RV stored at 25 °C and 4 °C are reported. Fig. 8 displays that the presence of RV stabilizes the quali-quantitative composition over time for both samples, thus maintaining a superimposable trend for the four main compounds for both storage conditions (Figs. 8 and 9).

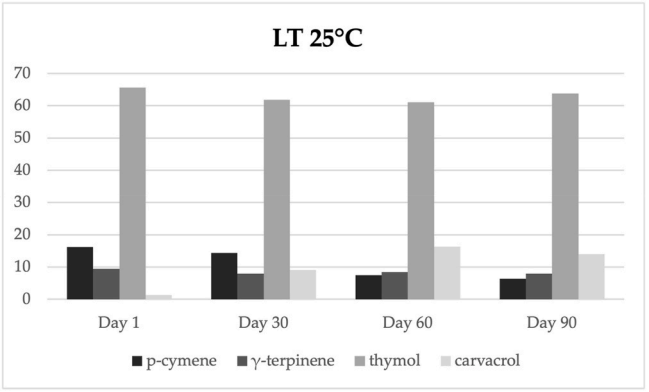

Fig. 6. Trend of the main components of LT (25 °C) over time.

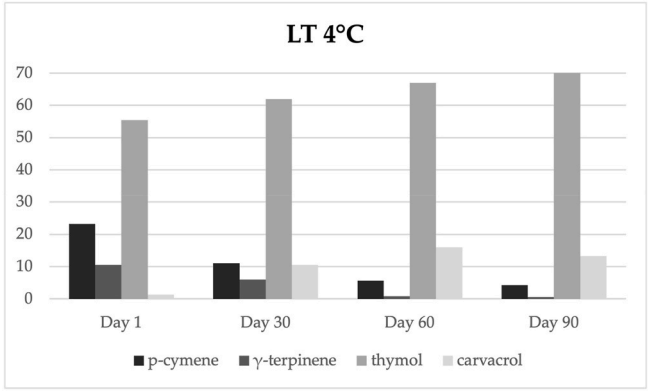

Fig. 7. Trend of the main components of LT (4 °C) over time.

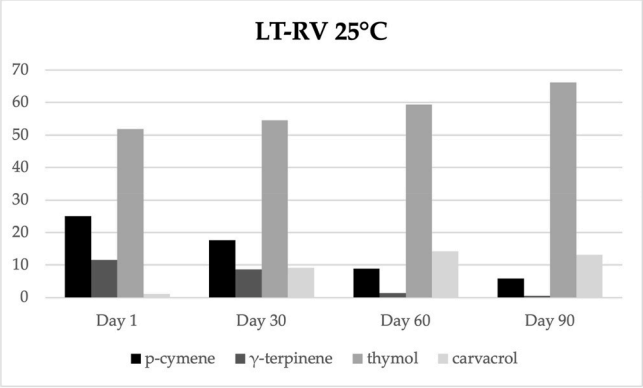

Fig. 8. Trend of the main components of LT-RV (25 °C) over time.

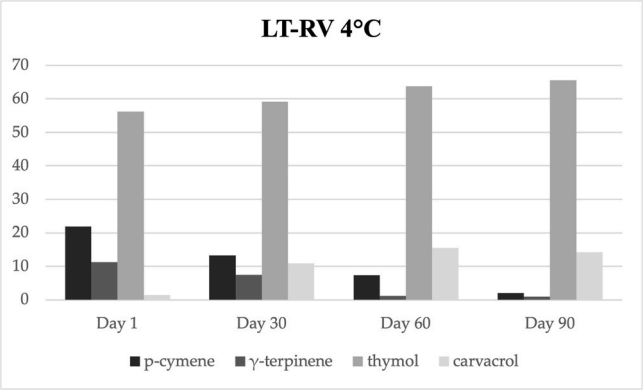

Fig. 9. Trend of the main components of LT-RV (4 °C) over time.

3.8. Resistance evaluation in culture media: DLS analysis

Stability studies on empty and RV-loaded samples in the culture media were conducted at 37 °C for 72 h, to highlight any changes in terms of HD. Nanocarriers do not behave as inert objects in solution; rather, they often undergo aggregation and/or agglomeration process, leading to the formation of a new range of multisized and unknown entities [61].

As shown in Fig. 10, both LT and LT-RV remain highly stable during the experiment in BHI and TSB. Only a slight increase in HD was observed at the end of the experiment probably due to the partial absorption on the liposome surface of proteins/salts. This behavior is less significant for LT-RV samples confirming the stabilizing effect of RV on the overall liposomal structure. These results confirm the stability of the samples in both media employed in biological evaluation.

3.9. In vitro release studies

The RV release experiment in Hepes buffer (Fig. 11) shows that the amount of RV released over 24 h is approximately 20 % of the initially loaded amount. The experiment was also carried out in culture media (until up to 72h) in order to obtain information about the vesicular resistance to the media employed in biological experiments. Similar trends were observed: in BHI and TBS, a maximum release of approximately 30 % was detected (Fig. S4).

The consistency of these findings indicates that the liposomal structures preserve their integrity in the tested environments. It is plausible that the multilamellar architecture, as evidenced by TEM, along with the specific bilayer properties revealed through fluorescence analyses, may act as a barrier to the full diffusion of RV into the surrounding medium.

3.10. MIC and MBC evaluation

The antimicrobial activity on the planktonic form of the different preparations was evaluated using a microdilution broth assay. A marked antibacterial activity of the liposomal preparations (LT and LT-RV) was observed (Table 4). The effect of EOs on bacteria is linked to different specific mechanisms of action such as degradation of the cell wall, damage to the cytoplasmic membrane, and damage to membrane proteins. This damage induces the leakage of the cell contents, the coagulation of the cytoplasm, and the depletion of the proton motive force, all causing cell death [62,63]. The anti-*Listeria* activity of thymol and carvacrol, components of TEO, was already demonstrated by several authors [64–66]. Notwithstanding the percentages of these compounds in LT-RV were higher than in LT, suggesting a potential stabilizing effect of RV on liposome composition, both formulations showed antimicrobial activity.

In line with this and in agreement with Motelica et al. (2023), who reported that nanoparticles loaded with TEO exhibited significant inhibitory activity against *L. monocytogenes*, our results further confirm the potential of thyme oil–based nanostructures as effective antibacterial systems against this pathogen [67].

For *L. monocytogenes* LM9, the MIC of LT-RV (65 μg/mL) was unexpectedly higher than that of LT (16 μg/mL). As reported by other authors, who studied the behavior of *L. monocytogenes* under different growth conditions, the bacterial cells tend to form aggregates when exposed to stress [68]. Similarly, we hypothesized that stress caused by LT-RV formulations might induce bacterial aggregation phenomena. Such aggregation may create a physical barrier that limits the ability of LT-RV to effectively reach and interact with individual planktonic bacterial cells.

Interestingly, free RV and LT-RV showed similar activity against *Listeria* spp. strains. Considering our results that demonstrated that approximately 30 % of the initially loaded quantity of RV was released from formulations, lead us to suppose a better antibacterial activity of LT-RV with respect to RV alone. Different studies reported RV

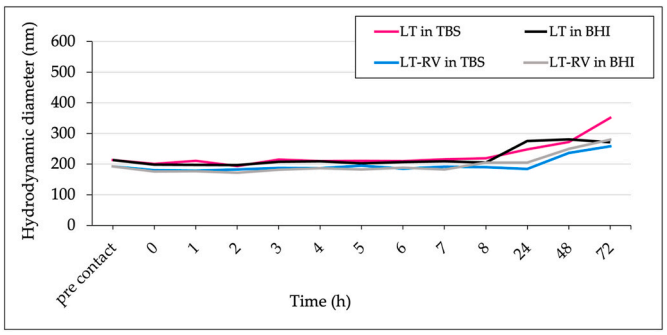

Fig. 10. Stability studies of LT and LT-RV in TBS and BHI culture media.

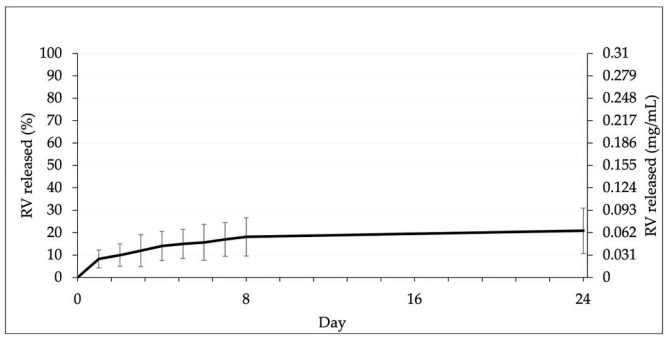

Fig. 11. Release studies of RV in Hepes buffer conducted at 37 °C for 24 h.

Table 4
MIC and MBC values of the strains treated with RV free or in LT/LT-RV. Results were expressed as μg/mL.

	LT		LT-RV		RV	
	MIC	MBC	MIC	MBC	MIC	MBC
***L. monocytogenes* (LM2)**	32.5	65	32.5	65	65	65
***L. monocytogenes* (LM9)**	16	65	65	130	32.5	65
***L. innocua* ATCC 1172**	65	65	65	130	65	65
***L. ivanovii* ATCC 19119**	65	65	65	65	65	65

antibacterial activities against foodborne pathogens including *L. monocytogenes*, by ATP synthase inhibition, DNA fragmentation, up-regulation of SOS stress response regulon and others. The same authors emphasized the development of delivery systems to improve RV physicochemical properties to enhance its therapeutic applicability [18,69,70].

3.11. Biofilm formation

The ability of microorganisms to produce biofilm was assessed using crystal violet staining according to the method of Stepanović et al., 2007 [38]. As already demonstrated by our research group [37], we confirmed that the amount of biofilm generated by LM2, that is a moderate biofilm producer, resulted lower than that of LM9, a strong biofilm producer. *L. innocua* ATCC 1172 and *L. ivanovii* ATCC 19119 were moderate and weak biofilm formers, respectively (Table 5).

3.12. Bacterial biofilm inhibition and eradication

The influence of sub-inhibiting concentrations of RV and different formulations on abilities of *Listeria* spp. strains to form or eradicate bacterial preformed biofilm was assayed, under static conditions, by crystal violet staining at 24 incubation time.

Interestingly, RV treatment inhibited biofilm formation of *L. innocua* ATCC 1172 strain and eradicated, at the same extent, mature biofilm also of clinical *L. monocytogenes* LM2 isolate. These data are in agreement with previous results demonstrating that RV strongly inhibited biofilm formation by both *L. innocua* and *L. monocytogenes* strains, even at subinhibitory concentrations [18].

As shown in Table 6, regardless of the different formation ability of the strains, sub-inhibiting concentrations of LT-RV were able to efficiently counteract the biofilm formation of all *Listeria* spp. strains respect LT. The most pronounced disruption of the EPS matrix induced by LT-RV, that affects both superficial and deeper layers, was also described by electron microscopy for *L. monocytogenes* LM9 strain in section 3.15.

The higher resistance of cells within mature biofilms was previously observed [71,72]. Actually, due to stronger three-dimensional structure, sessile protected cells in biofilm are more tolerant to stressful conditions and they can inactivate antimicrobial molecules [73,74].

As described above, the concentration of the most abundant component, thymol, was used for the EE% studies. Our results suggesting a potential stabilizing effect of RV on the liposome composition and indicating a higher retention of TEO in the presence of RV leads us to suppose an important contribution of TEO in the inhibition of *Listeria* spp. biofilm formation. Furthermore, in contrast to that observed for planktonic cells, considering the EE and release studies, a better inhibitory efficiency of LT-RV, with respect to free compounds, on bacterial sessile growth was demonstrated.

In this research, we remarked that whereas LT-RV showed, although with less efficiency, also an ability to eradicate preformed biofilm, neither 10 μg/mL nor 5 μg/mL of LT-RV destroyed mature biofilm of strong biofilm producer LM9 strain, highlighting strain-specific responses to the treatments (Table 7).

Table 5
Biofilm production of *Listeria* spp. strains.

Bacterial strains	Biofilm production
L. monocytogenes (LM2)	MODERATE
L. monocytogenes (LM9)	STRONG
L. innocua ATCC 1172	WEAK
L. ivanovii ATCC 19119	MODERATE

3.13. Morphological features of Listeria monocytogenes biofilm in the control Sample

The antimicrobial efficacy of LT-RV against *L. monocytogenes* strong biofilm producer LM9 strain biofilm formation was also validated through morphological examination conducted with SEM (Fig. 12).

The untreated *L. monocytogenes* biofilm (Fig. 12A) exhibits a polymeric extracellular matrix (EPS) organized into two distinct layers: a dense and compact surface layer and a trabeculated deeper layer with interconnected labyrinthine canaliculi. The surface layer is characterized by spherical-shaped irregularities with a rough texture, indicative of a well-structured biofilm.

3.14. Effect of TEO on Listeria monocytogenes biofilm

The *L. monocytogenes* biofilm treated with free TEO (Fig. 12B) exhibits significant structural disintegration. The outermost EPS layer appears strongly fragmented, losing its initial compactness. The underlying trabecular layer also shows visible erosion, with an irregular surface interspersed with numerous small, dispersed EPS clumps, suggesting a substantial breakdown of the biofilm matrix.

3.15. Effect of free RV on Listeria monocytogenes biofilm

The control sample, depicted in Fig. 13 A, shows a dense and compact EPS matrix with free bacterial cells (yellow) and partially embedded bacterial cells (pink) distributed within the biofilm structure. Fig. 13B illustrates the effects of free RV, where the outer surface remains dense, but develops thin streak-like formations, giving it a micro-network appearance. A free bacterial cell is also observed on the biofilm surface, suggesting localized structural alterations.

3.16. Effect of LT on Listeria monocytogenes biofilm

Treatment with LT (Fig. 13 C) induces moderate biofilm alterations. The superficial EPS layer (blue) appears less disrupted compared to the effects observed with free TEO. Although some degree of biofilm disintegration is present, the overall structure remains relatively intact, indicating a weaker destabilizing effect than TEO.

3.17. Effect of LT-RV on Listeria monocytogenes biofilm

Fig. 13D, E, and F illustrate the impact of LT-RV on *L. monocytogenes* biofilm. This treatment demonstrates the most pronounced disruption of the EPS matrix, affecting both superficial and deeper layers. As seen in Fig. 13D, the EPS is completely fragmented into micrometer-sized, coarsely spherical units. Higher magnification images (Fig. 13E and F) reveal a further breakdown of these structures into granular subunits of nanometer size with an irregular surface texture. Additionally, Listeria bacterial cells are visible within the disrupted biofilm, emphasizing the extensive structural alterations induced by LT-RV treatment.

•(

3.18. Summary of biofilm modifications induced by different treatments

A comparative analysis of the control and treated biofilms highlights

Table 6
Inhibition of biofilm formation by free RV or in LT and LT-RV. The results are expressed as percentages ± standard deviation (SD) values greater than 40 % were considered significant (in bold).

	LT 10 μg/mL	LT 5 μg/mL	LT–RV 10 μg/mL	LT-RV 5 μg/mL	RV 10 μg/mL	RV 5 μg/mL
***L. monocytogenes* (LM2)**	0.0 ± 0.1	11.7 ± 0.2	**93.1** ± 0.1	**54.5** ± 1.5	0.0 ± 0.3	1.5 ± 0.1
***L. monocytogenes* (LM9)**	0.0 ± 0.4	6.0 ± 1.1	**95.7** ± 0.1	**93.3** ± 0.5	0.0 ± 0.7	0.0 ± 0.7
***L. innocua* ATCC 1172**	17.8 ± 0.2	15.4 ± 0.7	**93.6** ± 0.1	**81.4** ± 0.2	0.0 ± 0.1	**43.1** ± 0.5
***L. ivanovii* ATCC 19119**	0.0 ± 0.5	5.0 ± 1.8	**97.7** ± 0.0	**88.2** ± 0.1	0.0 ± 0.2	20.5 ± 0.3

Table 7
Eradication of biofilm formation by free RV or LT and LT-RV. The results are expressed as percentages and values greater than 40 % were considered significant (in bold).

	LT 10 μg/mL	LT 5 μg/mL	LT–RV 10 μg/mL	LT-RV 5 μg/mL	RV 10 μg/mL	RV 5 μg/mL
***L. monocytogenes* (LM2)**	0.0 ± 0.0	0.0 ± 0.0	0.0 ± 0.4	**59.0** ± 7.6	**42.5** ± 0.3	**99.0** ± 0.5
***L. monocytogenes* (LM9)**	0.0 ± 0.0	0.0 ± 0.0	0.0 ± 0.0	0.0 ± 0.0	0.0 ± 0.6	0.0 ± 0.3
***L. innocua* ATCC 1172**	**51.0** ± 1.5	**54.0** ± 6.9	**66.5** ± 1.9	**68.0** ± 2.3	39.0 ± 0.4	**55.0** ± 0.6
***L. ivanovii* ATCC 19119**	34.5 ± 3.7	34.5 ± 2.0	**52.5** ± 0.5	**41.0** ± 1.8	20.5 ± 2.6	38.0 ± 0.2

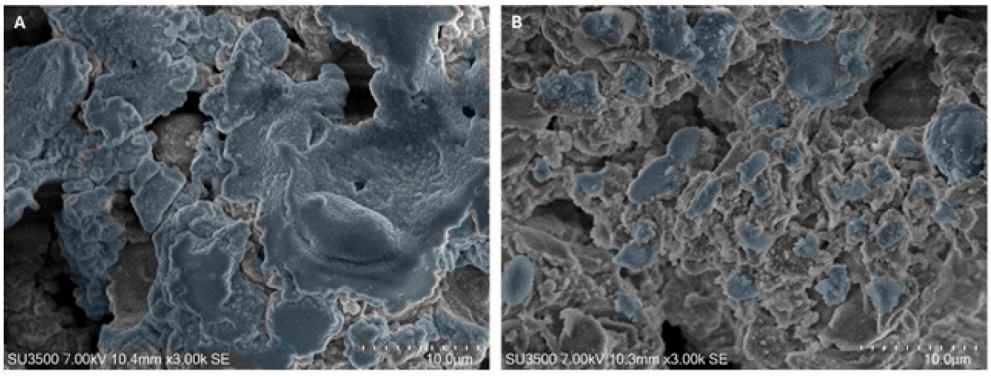

Fig. 12. Scanning electron micrographs of *L. monocytogenes* biofilm in control and free TEO-treated samples. (A) Control biofilm exhibiting a EPS with a dense and compact surface layer and a trabeculated deeper layer containing labyrinthine canaliculi. The surface is characterized by spherical-shaped irregularities with a rough texture, indicative of a well-structured biofilm. (B) Listeria biofilm treated with free TEO, showing severe fragmentation of the outermost EPS layer. The underlying trabecular structure is eroded, with an irregular surface dotted with numerous small EPS clumps, suggesting extensive biofilm disintegration.

differential structural alterations depending on the treatment applied. While free TEO and LT-RV exhibit the most pronounced biofilm-disrupting effects, LT and free RV cause moderate structural modifications, with LT displaying a weaker effect on EPS degradation. The most significant impact is observed with LT-RV, which completely disrupts the biofilm architecture, leading to a highly fragmented and granular EPS.

4. Conclusions

This study successfully optimized, prepared and characterized vesicular nanocarriers incorporating TEO and RV, thus demonstrating the added value of their combined use. This goal was achieved by applying advanced analytical techniques through a multidisciplinary approach. These methods are essential for fully understanding the structure and efficacy of bioactive-loaded liposomes.

The LT-RV system exhibited superior physicochemical stability compared to LT alone, with a reduced size increase over three months (from 181 ± 8 nm for LT to 176 ± 2 nm for LT-RV, $p < 0.05$) and a higher TEO retention efficiency (EE% 41 % in LT-RV vs. 35 % in LT). Additionally, anisotropy measurements indicated that RV confers increased bilayer rigidity, accounting for the long-term stability of LT-RV.

The production method preserved most of the active TEO components, as testified by the biological assays. LT-RV outperformed both free RV and LT. At sub-MIC concentrations (5–10 μg/mL), LT-RV achieved more than 40 % inhibition of *Listeria monocytogenes* biofilm formation, whereas LT or RV alone produced only moderate effects. SEM analysis confirmed that LT-RV caused the most extensive extracellular polymeric substance (EPS) disruption, fragmenting the biofilm matrix into nanometer-sized units and exposing bacterial cells, a result not observed with free RV or LT. The amount and stability of entrapped oil likely contribute to this improved performance. The present dual-loading strategy simultaneously preserves oil composition, stabilizes liposomal architecture, and enhances antimicrobial performance. Meanwhile, volatility and instability issues of essential oils can be overcome, while boosting bioactivity and reducing cytotoxicity.

Future research will focus on improving RV encapsulation efficiency beyond the current 25 %, elucidating the molecular mechanisms underlying biofilm inhibition, and validating the efficacy of LT-RV in real food matrices and *in vivo* models.

CRediT authorship contribution statement

Maria Gioia Fabiano: Writing – review & editing, Writing – original draft, Methodology, Investigation, Data curation, Conceptualization.

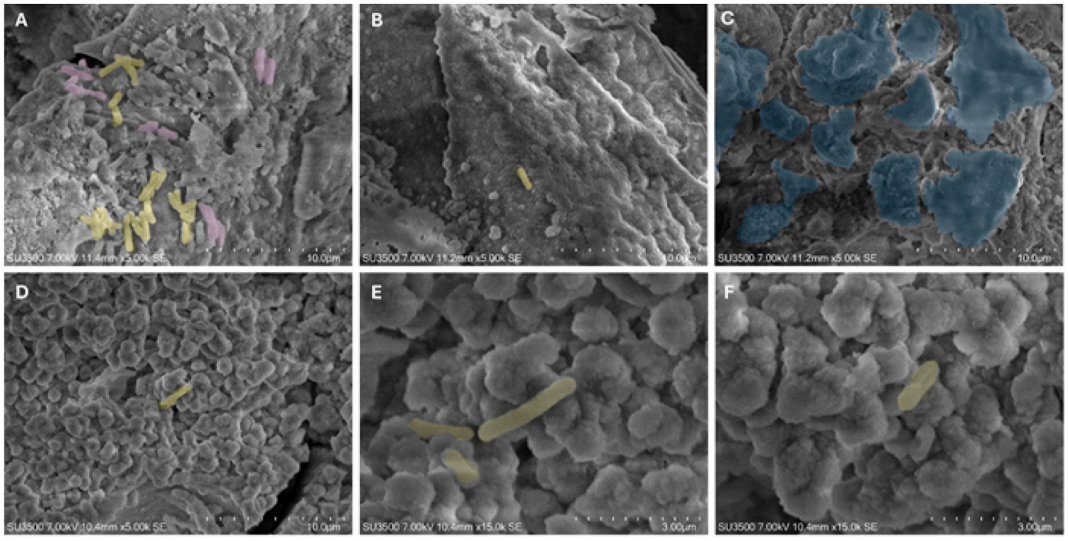

Fig. 13. Scanning electron micrographs of *L. monocytogenes* biofilm under different treatment conditions.
(A) Control biofilm with dense and compact EPS, displaying free bacterial cells (yellow) and partially embedded bacterial cells (pink) within the matrix.
(B) Biofilm treated with free RV, showing a dense outer layer with the formation of thin streak-like structures, creating a micro-network appearance. A free bacterial cell is visible on the biofilm surface.
(C) Biofilm treated with LT. The EPS surface layer (blue) exhibits partial disruption, but the overall structure remains relatively intact, indicating a weaker biofilm destabilization effect.
(D, E, F) Biofilm treated with LT-RV, showing the most significant EPS disintegration. (For interpretation of the references to colour in this figure legend, the reader is referred to the Web version of this article.)

Linda Maurizi: Writing – review & editing, Writing – original draft, Methodology, Investigation, Data curation, Conceptualization. **Jacopo Forte:** Investigation, Data curation. **Eleonora D'Intino:** Investigation, Data curation. **Maria Grazia Ammendolia:** Investigation, Formal analysis, Data curation. **Davide Corinti:** Writing – review & editing, Methodology, Investigation. **Astri D. Tagueha:** Writing – review & editing, Methodology, Investigation. **Michela Relucenti:** Writing – review & editing, Investigation, Data curation, Conceptualization. **Orlando Donfrancesco:** Methodology, Investigation. **Federica Rinaldi:** Writing – review & editing, Writing – original draft, Supervision, Investigation, Data curation, Conceptualization. **Maria Elisa Crestoni:** Writing – review & editing, Writing – original draft, Supervision, Funding acquisition, Data curation, Conceptualization. **Stefania Garzoli:** Writing – review & editing, Writing – original draft, Validation, Supervision, Conceptualization. **Carlotta Marianecci:** Writing – review & editing, Writing – original draft, Validation, Supervision, Conceptualization. **Maria Carafa:** Writing – review & editing, Writing – original draft, Validation, Supervision, Conceptualization. **Catia Longhi:** Writing – review & editing, Writing – original draft, Validation, Supervision, Conceptualization.

Declaration of competing interest

The authors declare that they have no known competing financial interests or personal relationships that could have appeared to influence the work reported in this paper.

Acknowledgment

This research was funded by PE00000003 (decree 1550, October 11, 2022) (“ON Foods – Research and innovation network on food and nutrition Sustainability, Safety and Security – Working ON Foods”) from the Italian Ministry of University and Research (Sapienza University CUP B53C22004030001) under the National Recovery and Resilience Plan (NRRP), funded by the European Union – NextGenerationEU.

Thanks to colleagues Daniela Scribano (Department of Public Health and Infectious Diseases, "Sapienza" University of Rome) and Cecilia Ambrosi (IRCCS San Raffaele Pisana, Department of Human Sciences and Promotion of the Quality of Life, San Raffaele Roma Open University, Rome, Italy) for their technical support.

Thanks to Tommy Cedervall's group (Department of Biochemistry and Structural Biology, Lund University) for allowing us to conduct the FT-IR analyses.

Appendix A. Supplementary data

Supplementary data to this article can be found online at https://doi.org/10.1016/j.jddst.2026.108027.

Data availability

Data will be made available on request.

References

[1] T.C. Ezike, U.S. Okpala, U.L. Onoja, C.P. Nwike, E.C. Ezeako, O.J. Okpara, C. C. Okoroafor, S.C. Eze, O.L. Kalu, E.C. Odoh, U.G. Nwadike, J.O. Ogbodo, B. U. Umeh, E.C. Ossai, B.C. Nwanguma, Advances in drug delivery systems, challenges and future directions, Heliyon 9 (2023) e17488, https://doi.org/10.1016/j.heliyon.2023.e17488.
[2] X. Shen, L. He, Y. Cui, Z. Lin, S.M. Jafari, C. Tan, Co-encapsulation of bioactive compounds in liposomal delivery systems for synergistic effects, Food Biosci. 68 (2025) 106306, https://doi.org/10.1016/j.fbio.2025.106306.
[3] E. Ganosi, C. Barda, M.-E. Grafakou, M.C. Rallis, H. Skaltsa, An In-Depth stability study of the essential oils from mentha × piperita, Mentha spicata, Origanum vulgare, and thymus vulgaris: the impact of thermal and storage conditions, Separations 10 (2023) 488, https://doi.org/10.3390/separations10090488.
[4] K. Etri, Z. Pluhár, Exploring chemical variability in the essential oils of the thymus genus, Plants 13 (2024) 1375, https://doi.org/10.3390/plants13101375.
[5] Y. Wu, N. Wan, Y. Liu, R.H. Lin, Y.T. Zhang, D.Y. Guo, J.B. Liao, T.H. Zhou, Z. F. Wu, M. Yang, Influencing factors, changing mechanisms and protection strategies of volatile oil from traditional Chinese medicine, Chin. Tradit. Herb. Drugs (2022) 6900–6908, https://doi.org/10.7501/j.issn.0253-2670.2022.21.029.
[6] V. Khwaza, B.A. Aderibigbe, Antibacterial activity of selected essential oil components and their derivatives: a review, Antibiotics 14 (2025) 68, https://doi.org/10.3390/antibiotics14010068.
[7] R.M. Senjab, N. AlSawaftah, W.H. Abuwatfa, G.A. Husseini, Advances in liposomal nanotechnology: from concept to clinics, RSC Pharmaceutics 1 (2024) 928–948, https://doi.org/10.1039/D4PM00176A.

[8] A. Kozak, E. Lavrih, G. Mikhaylov, B. Turk, O. Vasiljeva, Navigating the clinical landscape of liposomal therapeutics in cancer treatment, Pharmaceutics 17 (2025) 276, https://doi.org/10.3390/pharmaceutics17020276.

[9] S. Tiryaki, M. Macit, I.E. Zemheri, P.A. Süt, G. Duman, D. Telci, Anticancer activity of soy lecithin-based curcumin in prostate cancer, J of Applied Polymer Sci (2025) e56816, https://doi.org/10.1002/app.56816.

[10] D. Lombardo, M.A. Kiselev, Methods of liposomes preparation: formation and control factors of versatile nanocarriers for biomedical and nanomedicine application, Pharmaceutics 14 (2022) 543, https://doi.org/10.3390/pharmaceutics14030543.

[11] C.M. Barreto Pinilla, N.A. Lopes, A. Brandelli, Chapter 4 - liposome-mediated encapsulation of antimicrobials and probiotics, in: C. Anandharamakrishnan, S. Dutta (Eds.), Liposomal Encapsulation in Food Science and Technology, Academic Press, 2023, pp. 65–86, https://doi.org/10.1016/B978-0-12-823935-3.00011-4.

[12] K. Goktas, D. Yalcin, C. Erdem, B.T. Bicakci, O. Bayraktar, Optimization of mucoadhesive oral films containing olive leaf extract and microencapsulated thyme essential oil with potential antimicrobial activity, Food Sci. Nutr. 13 (2025) e4603, https://doi.org/10.1002/fsn3.4603.

[13] A. Kowalczyk, M. Przychodna, S. Sopata, A. Bodalska, I. Fecka, Thymol and thyme essential oil—new insights into selected therapeutic applications, Molecules 25 (2020) 4125, https://doi.org/10.3390/molecules25184125.

[14] C. Cimino, O.M. Maurel, T. Musumeci, A. Bonaccorso, F. Drago, E.M.B. Souto, R. Pignatello, C. Carbone, Essential oils: pharmaceutical applications and encapsulation strategies into lipid-based delivery systems, Pharmaceutics 13 (2021) 327, https://doi.org/10.3390/pharmaceutics13030327.

[15] M. Vestergaard, H. Ingmer, Antibacterial and antifungal properties of resveratrol, Int. J. Antimicrob. Agents 53 (2019) 716–723, https://doi.org/10.1016/j.ijantimicag.2019.02.015.

[16] X. Yu, Y. Jia, F. Ren, Multidimensional biological activities of resveratrol and its prospects and challenges in the health field, Front. Nutr. 11 (2024) 1408651, https://doi.org/10.3389/fnut.2024.1408651.

[17] A.R. Neves, M. Lucio, J.L.C. Lima, S. Reis, Resveratrol in medicinal chemistry: a critical review of its pharmacokinetics, drug-delivery, and membrane interactions, Curr. Med. Chem. 19 (2012) 1663–1681, https://doi.org/10.2174/092986712799945085.

[18] S. Ferreira, F. Domingues, The antimicrobial action of resveratrol against Listeria monocytogenes in food-based models and its antibiofilm properties, J. Sci. Food Agric. 96 (2016) 4531–4535, https://doi.org/10.1002/jsfa.7669.

[19] M. Sienkiewicz, M. Łysakowska, P. Denys, E. Kowalczyk, The antimicrobial activity of thyme essential oil against multidrug resistant clinical bacterial strains. https://Home.Liebertpub.Com/Mdr, 2012. https://doi.org/10.1089/mdr.2011.0080.

[20] A. Ed-Dra, L. Nalbone, A.A. Shahat, S. Laaraj, A. Farihi, S. Moujane, O.M. Noman, K. Elfazazi, A. Giuffrida, F. Giarratana, Antilisterial activity of *Thymus vulgaris* essential oil: *in vitro, in situ*, and *In silico* investigations, Microb. Pathog. 204 (2025) 107557, https://doi.org/10.1016/j.micpath.2025.107557.

[21] A.C. Santos, I. Pereira, M. Pereira-Silva, L. Ferreira, M. Caldas, M. Collado-González, M. Magalhães, A. Figueiras, A.J. Ribeiro, F. Veiga, Nanotechnology-based formulations for resveratrol delivery: effects on resveratrol in vivo bioavailability and bioactivity, Colloids Surf. B Biointerfaces 180 (2019) 127–140, https://doi.org/10.1016/j.colsurfb.2019.04.030.

[22] S. Armenta, S. Garrigues, F.A. Esteve-Turrillas, M. de la Guardia, Green extraction techniques in green analytical chemistry, TrAC, Trends Anal. Chem. 116 (2019) 248–253, https://doi.org/10.1016/j.trac.2019.03.016.

[23] M. Huq, M. Tascon, E. Nazdrajic, A. Roszkowska, J. Pawliszyn, Measurement of free drug concentration from biological tissue by solid-phase microextraction: in silico and experimental Study, Anal. Chem. 91 (2019) 7719–7728, https://doi.org/10.1021/acs.analchem.9b00983.

[24] C. Bicchi, M. Maffei, The plant volatilome: methods of analysis, in: J. Normanly (Ed.), High-Throughput Phenotyping in Plants: Methods and Protocols, Humana Press, Totowa, NJ, 2012, pp. 289–310, https://doi.org/10.1007/978-1-61779-995-2_15.

[25] L.T. Matereke, A.I. Okoh, Listeria monocytogenes virulence, antimicrobial resistance and environmental persistence: a review, Pathogens 9 (2020) 528, https://doi.org/10.3390/pathogens9070528.

[26] B. Lakicevic, I. Nastasijevic, *Listeria monocytogenes* in retail establishments: contamination routes and control strategies, Food Rev. Int. 33 (2017) 247–269, https://doi.org/10.1080/87559129.2016.1175017.

[27] P. Shree, C.K. Singh, K.K. Sodhi, J.N. Surya, D.K. Singh, Biofilms: understanding the structure and contribution towards bacterial resistance in antibiotics, Medicine in Microecology 16 (2023) 100084, https://doi.org/10.1016/j.medmic.2023.100084.

[28] J. Forte, P.N. Hanieh, N. Poerio, T. Olimpieri, M.G. Ammendolia, M. Fraziano, M. G. Fabiano, C. Marianecci, M. Carafa, F. Bordi, S. Sennato, F. Rinaldi, Mucoadhesive Rifampicin-Liposomes for the treatment of pulmonary infection by Mycobacterium abscessus: Chitosan or ε-Poly-L-Lysine decoration, Biomolecules 13 (2023) 924, https://doi.org/10.3390/biom13060924.

[29] D.E. Koppel, Analysis of macromolecular polydispersity in intensity correlation spectroscopy: the method of cumulants, J. Chem. Phys. 57 (1972) 4814–4820, https://doi.org/10.1063/1.1678153.

[30] R.J. Hunter, Zeta Potential in Colloid Science: Principles and Applications, Academic Press, 2013.

[31] W.T. Mason, Fluorescent and Luminescent Probes for Biological Activity: a Practical Guide to Technology for Quantitative Real-Time Analysis, Elsevier, 1999.

[32] S.-H. Park, S.-G. Oh, J.-Y. Mun, S.-S. Han, Effects of silver nanoparticles on the fluidity of bilayer in phospholipid liposome, Colloids Surf. B Biointerfaces 44 (2005) 117–122, https://doi.org/10.1016/j.colsurfb.2005.06.002.

[33] H. Jiang, Y. Wang, X. Xu, L. Deng, L. Feng, J. Han, W. Liu, Effect of oligosaccharides as lyoprotectants on the stability of curcumin-loaded nanoliposomes during lyophilization, Food Chem. 410 (2023) 135436, https://doi.org/10.1016/j.foodchem.2023.135436.

[34] F. Rinaldi, P.N. Hanieh, L.K.N. Chan, L. Angeloni, D. Passeri, M. Rossi, J.T.-W. Wang, A. Imbriano, M. Carafa, C. Marianecci, Chitosan glutamate-coated niosomes: a proposal for nose-to-brain delivery, Pharmaceutics 10 (2018) 38, https://doi.org/10.3390/pharmaceutics10020038.

[35] H. Hajimehdipoor, M. Shekarchi, M. Khanavi, N. Adib, M. Amri, A validated high performance liquid chromatography method for the analysis of thymol and carvacrol in Thymus vulgaris L. volatile oil, Pharmacogn. Mag. 6 (2010) 154–158, https://doi.org/10.4103/0973-1296.66927.

[36] T.L. Moore, L. Rodriguez-Lorenzo, V. Hirsch, S. Balog, D. Urban, C. Jud, B. Rothen-Rutishauser, M. Lattuada, A. Petri-Fink, Nanoparticle colloidal stability in cell culture media and impact on cellular interactions, Chem. Soc. Rev. 44 (2015) 6287–6305, https://doi.org/10.1039/C4CS00487F.

[37] M.G. Ammendolia, F. Iosi, B. De Berardis, G. Guccione, F. Superti, M.P. Conte, C. Longhi, Listeria monocytogenes behaviour in presence of Non-UV-Irradiated Titanium dioxide nanoparticles, PLoS One 9 (2014) e84986, https://doi.org/10.1371/journal.pone.0084986.

[38] S. Stepanović, D. Vuković, V. Hola, G.D. Bonaventura, S. Djukić, I. Ćirković, F. Ruzicka, Quantification of biofilm in microtiter plates: overview of testing conditions and practical recommendations for assessment of biofilm production by staphylococci, APMIS 115 (2007) 891–899, https://doi.org/10.1111/j.1600-0463.2007.apm_630.x.

[39] S. Stepanovic, I. Cirkovic, L. Ranin, M. Svabic-Vlahovic, Biofilm formation by Salmonella spp. and Listeria monocytogenes on plastic surface, Lett. Appl. Microbiol. 38 (2004) 428–432, https://doi.org/10.1111/j.1472-765X.2004.01513.x.

[40] M. Relucenti, G. Familiari, O. Donfrancesco, M. Taurino, X. Li, R. Chen, M. Artini, R. Papa, L. Selan, Microscopy methods for biofilm imaging: focus on SEM and VP-SEM pros and cons, Biology 10 (2021) 51, https://doi.org/10.3390/biology10010051.

[41] L. Maurizi, J. Forte, M.G. Ammendolia, P.N. Hanieh, A.L. Conte, M. Relucenti, O. Donfrancesco, C. Ricci, F. Rinaldi, C. Marianecci, M. Carafa, C. Longhi, Effect of ciprofloxacin-loaded niosomes on Escherichia coli and Staphylococcus aureus biofilm Formation, Pharmaceutics 14 (2022) 2662, https://doi.org/10.3390/pharmaceutics14122662.

[42] A. Akbarzadeh, R. Rezaei-Sadabady, S. Davaran, S.W. Joo, N. Zarghami, Y. Hanifehpour, M. Samiei, M. Kouhi, K. Nejati-Koshki, Liposome: classification, preparation, and applications, Nanoscale Res. Lett. 8 (2013) 102, https://doi.org/10.1186/1556-276X-8-102.

[43] M. Danaei, M. Dehghankhold, S. Ataei, F. Hasanzadeh Davarani, R. Javanmard, A. Dokhani, S. Khorasani, M.R. Mozafari, Impact of particle size and polydispersity index on the clinical applications of lipidic nanocarrier systems, Pharmaceutics 10 (2018) 57, https://doi.org/10.3390/pharmaceutics10020057.

[44] P. Foroozandeh, A.A. Aziz, Insight into cellular uptake and intracellular trafficking of nanoparticles, Nanoscale Res. Lett. 13 (2018) 339, https://doi.org/10.1186/s11671-018-2728-6.

[45] T.L. Nguyen, T.H. Nguyen, D.H. Nguyen, Development and in vitro evaluation of liposomes using soy lecithin to encapsulate Paclitaxel, International Journal of Biomaterials 2017 (2017) 8234712, https://doi.org/10.1155/2017/8234712.

[46] B.D. Isailović, I.T. Kostić, A. Zvonar, V.B. Đorđević, M. Gašperlin, V.A. Nedović, B. M. Bugarski, Resveratrol loaded liposomes produced by different techniques, Innov. Food Sci. Emerg. Technol. 19 (2013) 181–189, https://doi.org/10.1016/j.ifset.2013.03.006.

[47] M. Renault–Mahieux, N. Mignet, J. Seguin, K. Alhareth, M. Paul, K. Andrieux, Co–encapsulation of flavonoids with anti–cancer drugs: a challenge ahead, Int. J. Pharm. 623 (2022) 121942, https://doi.org/10.1016/j.ijpharm.2022.121942.

[48] D. Istrati, I. Lacatusu, N. Bordei, G. Badea, O. Oprea, L.M. Stefan, R. Stan, N. Badea, A. Meghea, Phyto-mediated nanostructured carriers based on dual vegetable actives involved in the prevention of cellular damage, Mater. Sci. Eng. C 64 (2016) 249–259, https://doi.org/10.1016/j.msec.2016.03.087.

[49] O.R. Bancuta, A. Chilian, I. Bancuta, R. Setnescu, T. Setnescu, R.M. Ion, Thermal characterization of resveratrol, Rev. Chim. 69 (2018) 1346–1351, https://doi.org/10.37358/RC.18.6.6322.

[50] K. Tai, F. Liu, X. He, P. Ma, L. Mao, Y. Gao, F. Yuan, The effect of sterol derivatives on properties of soybean and egg yolk lecithin liposomes: stability, structure and membrane characteristics, Food Res. Int. 109 (2018) 24–34, https://doi.org/10.1016/j.foodres.2018.04.014.

[51] S. Qayyum, A. Jabeen, Z. Aslam, T. Kanwal, M.R. Shah, S. Faizi, Synthesis and characterization of novel Lecithin derived nano-formulation of octyl and dodecyl gallate for targeting B cell associated non-hodgkin's lymphoma, J Clust Sci 34 (2023) 1369–1379, https://doi.org/10.1007/s10876-022-02302-w.

[52] S. Mohamadi, Z. Esfandiari, M. Khodadadi, M.S.T. Dehaghani, Simultaneous analysis of benzoic and sorbic acids in orange juice using thymol/water natural deep eutectic solvent and DLLME method followed by high performance liquid chromatography, Food Measure 18 (2024) 6285–6294, https://doi.org/10.1007/s11694-024-02647-y.

[53] Y. Li, K. Sun, S. Chen, J. Zhao, Y. Lei, L. Geng, Nano-Resveratrol liposome: physicochemical stability, in vitro release, and cytotoxicity, Appl. Biochem. Biotechnol. 195 (2023) 5950–5965, https://doi.org/10.1007/s12010-023-04344-w.

[54] N. Gan, Q. Li, Y. Li, M. Li, Y. Li, L. Chen, T. Zeng, Y. Song, F. Geng, D. Wu, Encapsulation of lemongrass essential oil by bilayer liposomes based on pectin, gum Arabic, and carrageenan: characterization and application in chicken meat preservation, Int. J. Biol. Macromol. 281 (2024) 135706, https://doi.org/10.1016/j.ijbiomac.2024.135706.
[55] D.Y. Chu, J.K. Thomas, Photophysical studies of molecular mobility in polymer films and bulk polymers. 3. Dynamic excimer formation of pyrene in bulk PDMS, Macromolecules 23 (1990) 2217–2222, https://doi.org/10.1021/ma00210a016.
[56] M. Koivusalo, J. Alvesalo, J.A. Virtanen, P. Somerharju, Partitioning of pyrene-labeled Phospho- and sphingolipids between ordered and disordered bilayer domains, Biophys. J. 86 (2004) 923–935, https://doi.org/10.1016/S0006-3495(04)74168-5.
[57] R. Gharib, L. Auezova, C. Charcosset, H. Greige-Gerges, Effect of a series of essential oil molecules on DPPC membrane fluidity: a biophysical study, J. Iran. Chem. Soc. 15 (2018) 75–84, https://doi.org/10.1007/s13738-017-1210-1.
[58] D.R. Khan, E.M. Rezler, J. Lauer-Fields, G.B. Fields, Effects of drug hydrophobicity on liposomal stability, Chem. Biol. Drug Des. 71 (2008) 3–7, https://doi.org/10.1111/j.1747-0285.2007.00610.x.
[59] R. Chelliah, I. Khan, E.B.-M. Daliri, L. Tamizhini, K.S. Pravitha, M. Begum, K. Saravanakumar, M.-H. Wang, D.H. Oh, Liposomes for drug delivery: progress and problems, in: J.-C. Kim, M. Alle, A. Husen (Eds.), Smart Nanomaterials in Biomedical Applications, Springer International Publishing, Cham, 2021, pp. 425–447, https://doi.org/10.1007/978-3-030-84262-8_15.
[60] E. Chibowski, A. Szcześ, Zeta potential and surface charge of DPPC and DOPC liposomes in the presence of PLC enzyme, Adsorption 22 (2016) 755–765, https://doi.org/10.1007/s10450-016-9767-z.
[61] G. Maiorano, S. Sabella, B. Sorce, V. Brunetti, M.A. Malvindi, R. Cingolani, P. P. Pompa, Effects of cell culture media on the dynamic Formation of protein−nanoparticle complexes and influence on the cellular response, ACS Nano 4 (2010) 7481–7491, https://doi.org/10.1021/nn101557e.
[62] K. Böhme, J. Barros-Velázquez, P. Calo-Mata, S.P. Aubourg, Antibacterial, antiviral and antifungal activity of essential oils: mechanisms and applications, in: T. G. Villa, P. Veiga-Crespo (Eds.), Antimicrobial Compounds: Current Strategies and New Alternatives, Springer, Berlin, Heidelberg, 2014, pp. 51–81, https://doi.org/10.1007/978-3-642-40444-3_3.
[63] S. Chouhan, K. Sharma, S. Guleria, Antimicrobial activity of some essential Oils—Present status and future perspectives, Medicines 4 (2017) 58, https://doi.org/10.3390/medicines4030058.
[64] S. Vidaković Knežević, S. Knežević, J. Vranešević, S.Ž. Kravić, B. Lakićević, S. Kocić-Tanackov, N. Karabasil, Effects of selected essential oils on Listeria monocytogenes in biofilms and in a model food System, Foods 12 (2023) 1930, https://doi.org/10.3390/foods12101930.
[65] G. Schneider, A. Steinbach, Á. Putics, Á. Solti-Hodován, T. Palkovics, Potential of essential oils in the control of Listeria monocytogenes, Microorganisms 11 (2023) 1364, https://doi.org/10.3390/microorganisms11061364.
[66] W. Churklam, S. Chaturongakul, B. Ngamwongsatit, R. Aunpad, The mechanisms of action of carvacrol and its synergism with nisin against *Listeria monocytogenes* on sliced bologna sausage, Food Control 108 (2020) 106864, https://doi.org/10.1016/j.foodcont.2019.106864.
[67] L. Motelica, B.-S. Vasile, A. Ficai, A.-V. Surdu, D. Ficai, O.-C. Oprea, E. Andronescu, G. Mustățea, E.L. Ungureanu, A.A. Dobre, Antibacterial activity of zinc oxide nanoparticles loaded with essential oils, Pharmaceutics 15 (2023) 2470, https://doi.org/10.3390/pharmaceutics15102470.
[68] O. Nwaiwu, L. Wong, M. Lad, T. Foster, W. MacNaughtan, C. Rees, Properties of the extracellular polymeric substance layer from minimally grown planktonic cells of Listeria monocytogenes, Biomolecules 11 (2021) 331, https://doi.org/10.3390/biom11020331.
[69] D.S.L. Ma, L.T.-H. Tan, K.-G. Chan, W.H. Yap, P. Pusparajah, L.-H. Chuah, L. C. Ming, T.M. Khan, L.-H. Lee, B.-H. Goh, Resveratrol—Potential antibacterial agent against foodborne pathogens, Front. Pharmacol. 9 (2018) 102, https://doi.org/10.3389/fphar.2018.00102.
[70] G.M. Dogheim, M.G. Shehat, D.M. Mahdy, H.S. Barakat, A. Abouelfetouh, A. A. Ramadan, Antibacterial and anti-virulence activity of eco-friendly resveratrol-loaded lipid nanocapsules against methicillin-resistant staphylococcus aureus, Sci. Rep. 15 (2025) 14677, https://doi.org/10.1038/s41598-025-95343-w.
[71] M. Sandasi, C.M. Leonard, A.M. Viljoen, The effect of five common essential oil components on *Listeria monocytogenes* biofilms, Food Control 19 (2008) 1070–1075, https://doi.org/10.1016/j.foodcont.2007.11.006.
[72] B.R.H. Cervantes-Huamán, A. Vega-Sánchez, P. Rolón-Verdún, G. Gervilla-Cantero, J.J. Rodríguez-Jerez, C. Ripolles-Avila, Effect of *Cinnamomum cassia* essential oil combined with enzymes on the elimination and regrowth potential of *Listeria monocytogenes* and *Salmonella enterica* biofilms formed on stainless steel surfaces, Food Control 172 (2025) 111120, https://doi.org/10.1016/j.foodcont.2024.111120.
[73] C. Uruén, G. Chopo-Escuin, J. Tommassen, R.C. Mainar-Jaime, J. Arenas, Biofilms as promoters of bacterial antibiotic resistance and tolerance, Antibiotics 10 (2020) 3, https://doi.org/10.3390/antibiotics10010003.
[74] S. Sharma, J. Mohler, S.D. Mahajan, S.A. Schwartz, L. Bruggemann, R. Aalinkeel, Microbial biofilm: a review on Formation, infection, antibiotic resistance, control measures, and innovative treatment, Microorganisms 11 (2023) 1614, https://doi.org/10.3390/microorganisms11061614.